Proceedings of the ASME 2010 3rd Joint US-European Fluids Engineering Summer Meeting and 8th International Conference on Nanochannels, Microchannels, and Minichannels
FEDSM-ICNMM2010
August 1-5, 2010, Montreal, Canada

FEDSM-ICNMM2010-31024

ADAPTIVE ANISOTROPIC STOCHASTIC DISCRETIZATION SCHEMES FOR UNCERTAIN CONSERVATION LAWS

Julie Tryoen *
Université Paris Est,
CERMICS, Ecole des Ponts,
77455 Marne la Vallée cedex 2,
France
Email: tryoenj@cermics.enpc.fr

Olivier Le Maître
LIMSI-CNRS (UPR3251),
91403 Orsay cedex,
France
Email: olm@limsi.fr

Alexandre Ern
Université Paris Est,
CERMICS, Ecole des Ponts,
77455 Marne la Vallée cedex 2,
France
Email: ern@cermics.enpc.fr

ABSTRACT

This paper deals with the design of adaptive anisotropic discretization schemes for conservation laws with stochastic parameters. A Finite Volume scheme is used for the deterministic discretization, while a piecewise polynomial representation is used at the stochastic level. The methodology is designed in the context of intrusive Galerkin projection methods with Roe-type solver. The adaptation aims at selecting the stochastic resolution level with regard to the local smoothness of the solution in the stochastic domain. In addition, the stochastic features of the solution greatly vary in the space and time so that the constructed stochastic approximation space depends on space and time. The overall method is assessed on the stochastic Burgers equation with shocks, showing significant computational savings.

INTRODUCTION

Stochastic spectral methods and so-called Chaos expansions provide effective tools for uncertainty quantification (UQ) and propagation in numerical models. The determination of the stochastic solution can be achieved by means of non intrusive (sampling based) methods or a stochastic Galerkin projection to derive a spectral problem for the stochastic modes; see, e.g., [1] and references therein. In this work, we consider the application of the Galerkin projection [2] to the resolution of conservation laws involving uncertain data (such as model parameters, initial and boundary conditions, and geometry) with known distribution functions. Previous applications of Galerkin projection to conservation laws include [3–7]. We are interested in problems where a shock appears almost surely in finite time. In this case, since the shock speed and/or its location in space can be uncertain, the solution is discontinuous in space and in the stochastic domain. This feature calls for specific discretization techniques. In particular, we rely on Finite Volume schemes for space discretization and on piecewise polynomial discretizations in the stochastic domain [8–10]. The use of piecewise polynomial representations helps prevent the emergence of Gibbs phenomena and aliasing errors associated with spectral representations based on smooth functions. In [7], we designed a Roe-type solver for the Galerkin system. Its key feature is an original technique to approximate efficiently the absolute value of the Galerkin Roe matrix based on evaluating a least-squares polynomial fitting the absolute value of the eigenvalues of the original stochastic hyperbolic problem at suitable collocation points. This solver was extensively tested in [7] on the stochastic Burgers and Euler equations and an entropy corrector was designed in [11].

The method proposed in [7], while able to deal with complex situations, remains expensive since a very fine stochastic discretization is needed to represent the solution in the neighborhood of discontinuities. This observation calls for adaptive strategies. Since discontinuities are localized in space and evolve in time, we propose in this work stochastic representations depending on space and time, meaning that, at a given time, each

*Address all correspondence to this author.

Finite Volume cell supports its own stochastic discretization. Consequently, the overall discretization does not rely on a tensorization of stochastic and deterministic approximation spaces, a feature which, to our knowledge, constitutes an original contribution of the present work. The above methodology can be formulated within a multiresolution framework based on the concept of general binary trees to describe the discretization of the stochastic domain, similarly to previous work in the deterministic context [12, 13]. The next ingredient is to allow for the adaptive enrichment and coarsening of the binary trees. In the present work, this is achieved using heuristic criteria where, in particular, the coarsening procedure relies on energy estimates. In addition, for multidimensional stochastic domains, an important feature of the present methodology is the anisotropy of the adaptive procedure.

The paper is organized as follows. First, we briefly recall the Galerkin projection of stochastic conservation laws and the Roe-type solver introduced in [7] in the non-adaptive context. Multiresolution analysis tools are then introduced together with suitable techniques for anisotropic adaptation in the context of uncertain conservation laws. Finally, simulations results are presented for the Burgers equation in two stochastic dimensions. Further development and testing of the present adaptive methodology for systems of uncertain conservation laws, such as the Euler equations, will be examined in future work.

GALERKIN PROJECTION AND ROE-TYPE SOLVER

Stochastic conservation laws

We are interested in stochastic nonlinear conservation laws with uncertain input quantities that can be parametrized for simplicity by N independent identically distributed random variables $\xi := \{\xi_1, \dots, \xi_{\mathrm{N}}\}$ uniformly distributed on $\Xi := [0,1]^{\mathrm{N}}$. Let us denote by $p_\xi = 1$ the density function of ξ and let $L^2(\Xi, p_\xi)$ be the space of second-order random variables defined on the probability space $\mathscr{P}_\xi := (\Xi, \mathscr{B}_\Xi, p_\xi)$, where $\mathscr{B}_\Xi$ is the Borel set of Ξ. The expectation operator in $\mathscr{P}_\xi$ is denoted for any random variable $H(\xi)$ defined on $\mathscr{P}_\xi$ by $\langle H \rangle := \int_\Xi H(y) p_\xi(y) \mathrm{d}y$. It is also possible to consider nonuniform random variables and to use an isoprobabilistic transformation to map them to uniform ones [9].

Let $(x,t,\xi) \in \Omega \times [0,T] \times \Xi$, where Ω is the spatial domain and T the simulation time. We seek for $U(x,t,\xi) \in \mathbb{R}^m \otimes L^2(\Xi, p_\xi)$, $m \geq 1$, solving almost surely the following conservative system

$$\begin{cases} \dfrac{\partial}{\partial t} U(x,t,\xi) + \dfrac{\partial}{\partial x} F(U(x,t,\xi);\xi) = 0, \\ U(x,t=0,\xi) = U_0(x,\xi), \end{cases} \tag{1}$$

where $F(U;\xi) \in \mathbb{R}^m \otimes L^2(\Xi, p_\xi)$ is the stochastic flux vector. The stochastic system (1) is assumed to be hyperbolic in the sense that the stochastic Jacobian matrix $\nabla_U F \in \mathbb{R}^{m,m} \otimes L^2(\Xi, p_\xi)$ is $\mathbb{R}$-diagonalizable almost surely.

Stochastic discretization

To approximate the solution in $L^2(\Xi, p_\xi)$, we need a stochastic discretization of the problem. This is obtained by considering a Hilbertian basis of random functionals in ξ spanning $L^2(\Xi, p_\xi)$,

$$L^2(\Xi, p_\xi) = \overline{span\{\Gamma_1(\xi), \Gamma_2(\xi), \dots\}}, \quad \langle \Gamma_\alpha \Gamma_\beta \rangle = \delta_{\alpha\beta}, \tag{2}$$

where $\delta_{\alpha\beta}$ denotes the Kronecker symbol. The discrete solution is sought in a finite dimensional subspace S^{P} of dimension P constructed by truncating the Hilbertian basis:

$$S^{\mathrm{P}} = span\{\Gamma_1(\xi), \Gamma_2(\xi), \dots, \Gamma_{\mathrm{P}}(\xi)\} \subset L^2(\Xi, p_\xi). \tag{3}$$

The approximate solution in S^{P} is expanded as a series in the form

$$U(x,t,\xi) \approx U^{\mathrm{P}}(x,t,\xi) = \sum_{\alpha=1}^{\mathrm{P}} u_\alpha(x,t) \Gamma_\alpha(\xi), \tag{4}$$

where the deterministic $\mathbb{R}^m$-valued fields $u_\alpha(x,t)$ are called the stochastic modes of the solution (in S^{P}).

The Galerkin system

Projecting (1) on the stochastic basis, we obtain the Galerkin system which couples all the stochastic modes in the form

$$\begin{cases} \dfrac{\partial}{\partial t} u(x,t) + \dfrac{\partial}{\partial x} f(u(x,t)) = 0, \\ u(x,t=0) = u^0(x), \end{cases} \tag{5}$$

where $u(x,t) = (u_1(x,t), \cdots, u_{\mathrm{P}}(x,t))^T \in \mathbb{R}^{m\mathrm{P}}$, and $f(u(x,t)) = (f_1(u), \cdots, f_{\mathrm{P}}(u))^T \in \mathbb{R}^{m\mathrm{P}}$ are respectively the vector of the stochastic modes and the Galerkin flux vector with

$$f_\alpha(u) := \left\langle \Gamma_\alpha F\left(U^{\mathrm{P}}; \cdot\right) \right\rangle \quad \text{and} \quad U^{\mathrm{P}} = \sum_{\beta=1}^{\mathrm{P}} u_\beta \Gamma_\beta(\xi). \tag{6}$$

Moreover, we take for the initial condition $u^0 = (\langle \Gamma_\alpha U_0 \rangle)_{\alpha=1,\dots,\mathrm{P}}$. The Galerkin Jacobian matrix $\nabla_u f$ of order $m\mathrm{P}$ is given by

$$(\nabla_u f(u))_{\alpha,\beta=1,\dots,\mathrm{P}} = \left\langle \nabla_U F(U^{\mathrm{P}}; \cdot) \Gamma_\alpha \Gamma_\beta \right\rangle_{\alpha,\beta=1,\dots,\mathrm{P}}. \tag{7}$$

The hyperbolicity of the Galerkin system (5), that is, the $\mathbb{R}$-diagonalizability of the Galerkin Jacobian matrix $\nabla_u f$, has been extensively studied in [7] (in fact, in the more general context of multiresolution analysis which will be introduced in the sequel). In particular, in the context of scalar conservation laws, as for the results shown below, the Galerkin system is proven to be hyperbolic.

Roe-type solver

The Galerkin system (5) is discretized in space and time using a Finite Volume method in the form

$$u_i^{n+1} = u_i^n - \frac{\Delta t^n}{\Delta x}\left(\varphi(u_i^n, u_{i+1}^n) - \varphi(u_{i-1}^n, u_i^n)\right), \tag{8}$$

where u_i^n is an approximation to the cell-average in the spatial domain of the solution u in the cell of center $x_i := i\Delta x$ with width Δx at the time discrete t^n and $\varphi(\cdot,\cdot)$ is the Galerkin numerical flux.

The Roe-type solver can be viewed as an approximate Riemann solver where the Galerkin flux $f(u)$ is replaced at each interface LR separating left and right states (u_L, u_R) by the linear approximation

$$f^{\mathrm{Roe}}(u_L, u_R, u) = f(u_L) + a(u_L, u_R)\cdot(u - u_L), \tag{9}$$

where $a(u_L, u_R)$ is a Roe-linearized approximation of the Galerkin Jacobian matrix. To define $a(u_L, u_R)$, we assume that the original stochastic problem (1) possesses a Roe state $U_{LR}^{\mathrm{Roe}}(\xi)$ on each interface LR separating left and right stochastic states $(U_L(\xi), U_R(\xi))$ such that $\nabla_U F(U_{LR}^{\mathrm{Roe}}(\xi))$ is a Roe linearized matrix for the stochastic problem. Then, for all $U_L^{\mathrm{P}}, U_R^{\mathrm{P}} \in \mathbb{R}^m \otimes S^{\mathrm{P}}$, letting $U_{LR}^{\mathrm{Roe}} \in \mathbb{R}^m \otimes L^2(\Xi, p_\xi)$ be the associated Roe state, we have proven in [7] that in the context of scalar conservation laws,

$$a_{LR}^{\mathrm{Roe}} := a(u_L, u_R) := \left\langle \nabla_U F(U_{LR}^{\mathrm{Roe}}; \cdot)\Gamma_\alpha \Gamma_\beta \right\rangle_{\alpha,\beta=1,\ldots,\mathrm{P}} \tag{10}$$

is a Roe linearized matrix for the Galerkin problem. The Galerkin numerical flux is chosen in the form

$$\varphi(u_L, u_R) := \varphi^{\mathrm{Roe}}(u_L, u_R) = \frac{f(u_L) + f(u_R)}{2} - |a_{LR}^{\mathrm{Roe}}|\,\frac{u_R - u_L}{2}. \tag{11}$$

However, to avoid the expensive spectral decomposition of the Roe Galerkin Jacobian matrix a_{LR}^{Roe} when computing its absolute value, we approximate $|a_{LR}^{\mathrm{Roe}}|$ by applying (using Hörner's method) a polynomial $q_{d_{\mathrm{fit}},\{\lambda'\}}$ to the Roe linearized matrix a_{LR}^{Roe}. The polynomial $q_{d_{\mathrm{fit}},\{\lambda'\}}$ is of degree $\leq d_{\mathrm{fit}}$ (fixed a priori) and is determined using an approximate spectrum $\{\lambda'_\gamma\}_{\gamma=1,\ldots,n_{\lambda'}}$ of a_{LR}^{Roe} and minimizing the least-squares error $\sum_{\gamma=1}^{n_{\lambda'}}\left(|\lambda'_\gamma| - q_{d_{\mathrm{fit}},\{\lambda'\}}(\lambda'_\gamma)\right)^2$. The approximate eigenvalues λ'_γ are taken as the stochastic eigenvalues of the original system evaluated at some collocative nodes. This procedure, while saving substantial computational times, implies that the underlying scheme is not, strictly speaking, a Roe scheme. However, detailed numerical studies reported in [7] confirm that the scheme works well in practice. Finally, the time-step Δt^n is computed using a CFL-type condition in the form

$$\frac{\Delta t^n}{\Delta x} = \frac{\mathrm{CFL}}{\max\limits_{LR\in\mathscr{I},\gamma=1,\ldots,n_{\lambda'}} |\lambda'_\gamma|}, \tag{12}$$

where $\mathscr{I}$ denotes the set of interfaces LR in the spatial domain and CFL denotes a user-dependent positive parameter ≤ 1.

MULTIRESOLUTION ANALYSIS

As motivated in the introduction, since shock velocities and shock location can be uncertain, the solution is not smooth in the stochastic domain. Consequently, as in [8–10], we rely on multiresolution analysis based on piecewise polynomial approximations. We first consider the one-dimensional stochastic case $\mathrm{N} = 1$; the multidimensional case is treated at the end of the section.

Complete binary trees

We discretize the stochastic space $\Xi = [0,1]$ using stochastic elements (intervals here), resulting from successive dyadic partitions of Ξ:

$$\Xi = \bigcup_{l\in\{1,\ldots,2^{\mathrm{Nr}}\}} \left[(l-1)2^{-\mathrm{Nr}}, l2^{-\mathrm{Nr}}\right], \tag{13}$$

where $\mathrm{Nr} \geq 0$ is the resolution level. A key feature which will be used in the design of adaptive schemes is that the partition of Ξ in (13) has a complete binary tree structure. The binary tree structure is illustrated in Figure 1 for the case $\mathrm{Nr} = 4$. We define for a binary tree $\mathscr{T}$:

the set of nodes: $\mathscr{N}(\mathscr{T})$,
the set of leafs: $\mathscr{L}(\mathscr{T}) \subset \mathscr{N}(\mathscr{T})$,
the parent of a node $\mathtt{n} \in \mathscr{N}(\mathscr{T})$: $\mathtt{p}(\mathtt{n})$,
the "left" and "right" children of a node $\mathtt{n} \in \mathscr{N}(\mathscr{T}) \setminus \mathscr{L}(\mathscr{T})$: $\mathtt{c}^-(\mathtt{n})$ and $\mathtt{c}^+(\mathtt{n})$,
the distance of a node $\mathtt{n} \in \mathscr{N}(\mathscr{T})$: $|\mathtt{n}|$,
the depth of the tree: $\mathrm{Nr}(\mathscr{T})$,
the support of a node $\mathtt{n} \in \mathscr{N}(\mathscr{T})$: $\mathscr{S}(\mathtt{n})$.

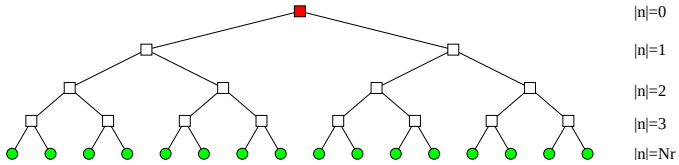

FIGURE 1. INTERPRETATION OF THE DYADIC PARTITION OF Ξ BY A COMPLETE BINARY TREE.

The root node of $\mathscr{T}$, located on top, is denoted $\mathtt{n}_0$. All nodes but the root have a unique parent. The distance $|\mathtt{n}|$ of a particular node is defined relatively to the root node; the root node $\mathtt{n}_0$ has a distance $|\mathtt{n}_0| = 0$ and its two children have a distance $|\mathtt{c}^-(\mathtt{n}_0)| = |\mathtt{c}^+(\mathtt{n}_0)| = 1$. The depth $\mathrm{Nr}(\mathscr{T})$ of a tree is the maximal distance over all the tree's nodes. A complete binary tree is such that a node $\mathtt{n}$ with $|\mathtt{n}| < \mathrm{Nr}(\mathscr{T})$ has two children; in a complete binary tree there are 2^d nodes $\mathtt{n}$ having distance $|\mathtt{n}| = d$, and the $2^{\mathrm{Nr}(\mathscr{T})}$ nodes with $|\mathtt{n}| = \mathrm{Nr}$ have no child and are called the leafs $\mathtt{l} \in \mathscr{L}(\mathscr{T})$. For more general binary tree structures (see below), a node with no child is called a leaf. The supports $\mathscr{S}(\mathtt{n})$ can be defined recursively. First, the support of the root node is $\mathscr{S}(\mathtt{n}_0) = [0,1]$ and letting $\mathscr{S}(\mathtt{n}) = [\xi_\mathtt{n}^-, \xi_\mathtt{n}^+]$ be the support of node $\mathtt{n}$, with $\mathtt{n} \notin \mathscr{L}(\mathscr{T})$, then the support of its left and right children are respectively $\mathscr{S}(\mathtt{c}^-(\mathtt{n})) = [\xi_\mathtt{n}^-, (\xi_\mathtt{n}^- + \xi_\mathtt{n}^+)/2]$ and $\mathscr{S}(\mathtt{c}^+(\mathtt{n})) = [(\xi_\mathtt{n}^- + \xi_\mathtt{n}^+)/2, \xi_\mathtt{n}^+]$. Therefore, an alternative expression for (13) is

$$\Xi = \bigcup_{\mathtt{l} \in \mathscr{L}(\mathscr{T})} \mathscr{S}(\mathtt{l}). \tag{14}$$

Multiresolution spaces

Consider a complete binary tree $\mathscr{T}$ with $\mathrm{Nr}(\mathscr{T}) \geq 0$. We denote by $S^{\mathrm{No}}(\mathscr{T}) := S^{\mathrm{P}}$ the stochastic approximation space consisting of piecewise polynomials in ξ,

$$S^{\mathrm{No}}(\mathscr{T}) = \{H : [0,1] \to \mathbb{R}; \forall \mathtt{l} \in \mathscr{L}(\mathscr{T}), H|_{\mathscr{S}(\mathtt{l})} \in \Pi_{\mathrm{No}}[\xi]\}, \tag{15}$$

where $\mathrm{No} \geq 0$ and $\Pi_{\mathrm{No}}[\xi]$ denotes the vector space of real polynomials with degree $\leq \mathrm{No}$ in ξ. Therefore, the space $S^{\mathrm{No}}(\mathscr{T})$ has dimension

$$\dim S^{\mathrm{No}}(\mathscr{T}) =: \mathrm{P}_\pi \,\mathrm{card}(\mathscr{L}(\mathscr{T})) =: \mathrm{P}(\mathscr{T}), \tag{16}$$

where $\mathrm{P}_\pi := (\mathrm{No}+1)$ is the dimension of the local polynomial basis on each leaf; we recall that $\mathrm{card}(\mathscr{L}(\mathscr{T})) = 2^{\mathrm{Nr}(\mathscr{T})}$ for a complete binary tree. The spaces $S^{\mathrm{No}}(\mathscr{T})$ form a hierarchical family of stochastic spaces since $S^{\mathrm{No}}(\mathscr{T}) \subseteq S^{\mathrm{No}'}(\mathscr{T})$ for $\mathrm{No} \leq \mathrm{No}'$ and $S^{\mathrm{No}}(\mathscr{T}) \subseteq S^{\mathrm{No}}(\mathscr{T}')$ for two complete binary trees such that $\mathrm{Nr}(\mathscr{T}) \leq \mathrm{Nr}(\mathscr{T}')$. We now introduce two bases for $S^{\mathrm{No}}(\mathscr{T})$.

Stochastic Element (SE) basis. A function H of $S^{\mathrm{No}}(\mathscr{T})$ can be expanded locally on each leaf $\mathtt{l} \in \mathscr{L}(\mathscr{T})$ using the $(\mathrm{No}+1)$ rescaled and normalized Legendre polynomials defined on $\mathscr{S}(\mathtt{l})$, such that any functional $H(\xi) \in L^2(\Xi, p_\xi)$ has for expansion on $S^{\mathrm{No}}(\mathscr{T})$,

$$H(\xi) \approx H^{\mathscr{T}}(\xi) = \sum_{\mathtt{l} \in \mathscr{L}(\mathscr{T})} \left(\sum_{\alpha=1}^{\mathrm{P}_\pi} h_\alpha^\mathtt{l} \Phi_\alpha^\mathtt{l}(\xi) \right), \tag{17}$$

where the deterministic coefficients $h_\alpha^\mathtt{l} \in \mathbb{R}$ are called the SE coefficients of H in $S^{\mathrm{No}}(\mathscr{T})$, and $\{\Phi_\alpha^\mathtt{l}\}_{\mathtt{l} \in \mathscr{L}(\mathscr{T}), \alpha=1,\ldots,\mathrm{P}_\pi}$ denotes the SE basis relative to the complete binary tree $\mathscr{T}$ for given expansion order No. Denoting $\{\Phi_\alpha^{\mathtt{n}_0}\}_{1 \leq \alpha \leq \mathrm{P}_\pi}$ the set of normalized Legendre polynomials on Ξ, the $\Phi_\alpha^\mathtt{l}$ have for expression

$$\Phi_\alpha^\mathtt{l}(\xi) = \begin{cases} \dfrac{1}{\sqrt{2^{-|\mathtt{l}|}}} \Phi_\alpha^{\mathtt{n}_0} \left(\dfrac{\xi - \xi_\mathtt{l}^-}{\xi_\mathtt{l}^+ - \xi_\mathtt{l}^-} \right), & \xi \in \mathscr{S}(\mathtt{l}) = [\xi_\mathtt{l}^-, \xi_\mathtt{l}^+], \\ 0, & \text{otherwise}, \end{cases} \tag{18}$$

and form an orthonormal set:

$$\left\langle \Phi_\alpha^\mathtt{l} \Phi_\beta^{\mathtt{l}'} \right\rangle = \delta_{\mathtt{l},\mathtt{l}'} \delta_{\alpha,\beta}, \; \forall \mathtt{l}, \mathtt{l}' \in \mathscr{L}(\mathscr{T}), \; 1 \leq \alpha, \beta \leq \mathrm{P}_\pi. \tag{19}$$

Relying on a multi-index $\mathbf{i}$, the SE expansion can be recast as

$$H(\xi) \approx H^{\mathscr{T}}(\xi) = \sum_{\mathbf{i} \in SE^{\mathrm{No}}(\mathscr{T})} h_\mathbf{i} \Phi_\mathbf{i}(\xi), \tag{20}$$

where $SE^{\mathrm{No}}(\mathscr{T})$ is the multi-index set of the SE expansion, with $\mathrm{card}\left(SE^{\mathrm{No}}(\mathscr{T})\right) = \mathrm{P}(\mathscr{T})$. If $H \in L^2(\Xi, p_\xi)$ is known, then $h_\mathbf{i} = \langle \Phi_\mathbf{i} H \rangle$ for all $\mathbf{i} \in SE^{\mathrm{No}}(\mathscr{T})$.

Multiwavelet (MW) basis. Alternatively, $S^{\mathrm{No}}(\mathscr{T})$ can be spanned by the hierarchical MW system of order No and resolution level Nr introduced in [9]. We recall here some details about the construction of the MW system. We consider the sequence of complete binary trees $\mathscr{T}_{[r]}$, $r = 0, 1, \ldots$, where the bracketed subscript refers to the resolution (depth) of the complete binary tree, so that $\mathrm{Nr}(\mathscr{T}_{[r]}) = r$. For $\mathrm{No} \geq 0$, let $W^{\mathrm{No}}(\mathscr{T}_{[r]})$ denote the detail space, that is, the $L^2(\Xi, p_\xi)$-orthogonal complement of $S^{\mathrm{No}}(\mathscr{T}_{[r]})$ in $S^{\mathrm{No}}(\mathscr{T}_{[r+1]})$:

$$S^{\mathrm{No}}(\mathscr{T}_{[r+1]}) = S^{\mathrm{No}}(\mathscr{T}_{[r]}) \oplus W^{\mathrm{No}}(\mathscr{T}_{[r]}). \tag{21}$$

As a result, for $\mathrm{Nr} \geq 0$,

$$S^{\mathrm{No}}(\mathscr{T}_{[\mathrm{Nr}]}) = S^{\mathrm{No}}(\mathscr{T}_{[0]}) \bigoplus_{r=0}^{\mathrm{Nr}-1} W^{\mathrm{No}}(\mathscr{T}_{[r]}). \tag{22}$$

The set of normalized Legendre polynomials, with degree $\leq \mathrm{No}$, is again used as a basis of $S^{\mathrm{No}}(\mathscr{T}_{[0]})$, that is,

$$S^{\mathrm{No}}(\mathscr{T}_{[0]}) = span\{\Phi_1^{\mathtt{n}_0}, \ldots, \Phi_{\mathrm{P}_\pi}^{\mathtt{n}_0}\}, \tag{23}$$

where $\mathtt{n}_0$ is the unique node of $\mathscr{T}_{[0]}$. We now seek for an orthonormal basis $\{\Psi_1, \ldots, \Psi_{\mathrm{P}_\pi}\}$ for $W^{\mathrm{No}}(\mathscr{T}_{[0]})$. Since $W^{\mathrm{No}}(\mathscr{T}_{[0]})$ and $S^{\mathrm{No}}(\mathscr{T}_{[0]})$ are $L^2(\Xi, p_\xi)$-orthogonal, the functions Ψ_α are such that

$$\left\langle \Psi_\alpha \Phi_\beta^{\mathtt{n}_0} \right\rangle = 0 \text{ and } \left\langle \Psi_\alpha \Psi_\beta \right\rangle = \delta_{\alpha,\beta},\ 1 \leq \alpha, \beta \leq \mathrm{P}_\pi. \tag{24}$$

In addition, the functions Ψ_α are piecewise polynomials on $[0, 1/2] \cup [1/2, 1]$ with degree $\leq \mathrm{No}$. The $2\mathrm{P}_\pi$ conditions in (24) define the functions Ψ_α, which are computed following the algorithm proposed by Alpert and co-workers in [14]. The resulting functions are depicted in Figure 2 for the polynomial orders $\mathrm{No} = 1$ and $\mathrm{No} = 3$. Once the funcitons Ψ_α are known, we can construct the basis for $W^{\mathrm{No}}(\mathscr{T}_{[r]})$ using rescaled and shifted versions of the basis vectors of $W^{\mathrm{No}}(\mathscr{T}_{[0]})$; indeed, defining

$$W^{\mathrm{No}}(\mathscr{T}_{[r]}) = span\{\Psi_\alpha^{\mathtt{l}};\ \mathtt{l} \in \mathscr{L}(\mathscr{T}_{[r]}),\ 1 \leq \alpha \leq \mathrm{P}_\pi\}, \tag{25}$$

where

$$\Psi_\alpha^{\mathtt{l}}(\xi) = \begin{cases} \dfrac{1}{\sqrt{2^{-|\mathtt{l}|}}} \Psi_\alpha\left(\dfrac{\xi - \xi_{\mathtt{l}}^-}{\xi_{\mathtt{l}}^+ - \xi_{\mathtt{l}}^-}\right), & \xi \in \mathscr{S}(\mathtt{l}) = [\xi_{\mathtt{l}}^-, \xi_{\mathtt{l}}^+], \\ 0, & \text{otherwise}, \end{cases} \tag{26}$$

it is immediate to verify that $\forall \mathtt{n}, \mathtt{n}' \in \mathscr{N}(\mathscr{T})$ and $1 \leq \alpha, \beta \leq \mathrm{P}_\pi$,

$$\left\langle \Psi_\alpha^{\mathtt{n}} \Phi_\beta^{\mathtt{n}_0} \right\rangle = 0, \quad \left\langle \Psi_\alpha^{\mathtt{n}} \Psi_\beta^{\mathtt{n}'} \right\rangle = \delta_{\mathtt{n},\mathtt{n}'} \delta_{\alpha,\beta}. \tag{27}$$

Hence, any functional $H(\xi) \in L^2(\Xi, p_\xi)$ has the following MW expansion on $S^{\mathrm{No}}(\mathscr{T})$:

$$H(\xi) \approx H^{\mathscr{T}}(\xi) = \sum_{\alpha=1}^{\mathrm{P}_\pi} h_\alpha^{\mathtt{n}_0} \Phi_\alpha^{\mathtt{n}_0}(\xi) + \sum_{\substack{\mathtt{n} \in \mathscr{N}(\mathscr{T}) \\ \mathtt{n} \notin \mathscr{L}(\mathscr{T})}} \left(\sum_{\alpha=1}^{\mathrm{P}_\pi} \tilde{h}_\alpha^{\mathtt{n}} \Psi_\alpha^{\mathtt{n}}(\xi) \right). \tag{28}$$

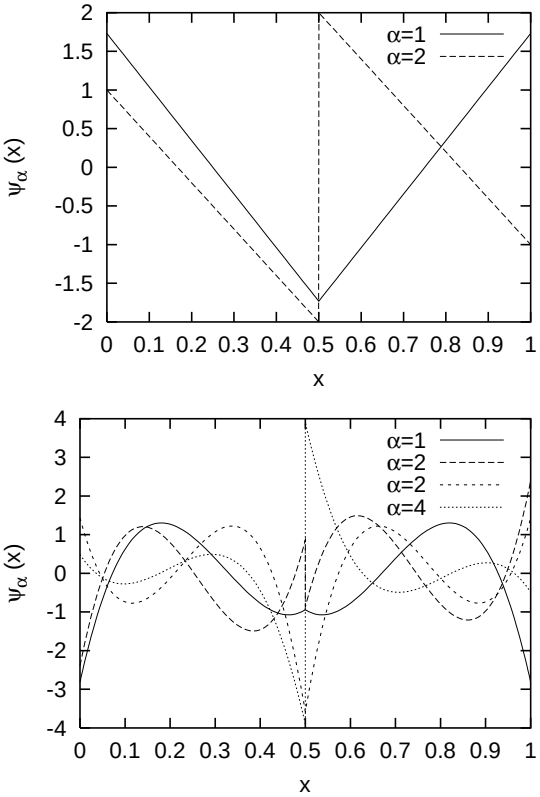

FIGURE 2. EXAMPLE OF FUNCTIONS Ψ_α SPANNING $W^{\mathrm{No}}(\mathscr{T}_{[0]})$ FOR $\mathrm{No} = 1$ (TOP) AND $\mathrm{No} = 3$ (BOTTOM).

Again, relying on a multi-index $\mathbf{i}$, the MW expansion can be recast as

$$H(\xi) \approx \tilde{H}^{\mathscr{T}}(\xi) = \sum_{\mathbf{i} \in MW^{\mathrm{No}}(\mathscr{T})} \tilde{h}_{\mathbf{i}} \Psi_{\mathbf{i}}(\xi), \tag{29}$$

where $MW^{\mathrm{No}}(\mathscr{T})$ is the multi-index set of the MW expansion, with $\mathrm{card}\left(MW^{\mathrm{No}}(\mathscr{T})\right) = \mathrm{P}(\mathscr{T})$. If $H(\xi) \in L^2(\Xi, p_\xi)$ is known, then $\tilde{h}_{\mathbf{i}} = \left\langle \Psi_{\mathbf{i}} \tilde{H} \right\rangle$ for all $\mathbf{i} \in MW^{\mathrm{No}}(\mathscr{T})$.

Finally, there is an orthogonal transition matrix $B \in \mathbb{R}^{\mathrm{P}(\mathscr{T}),\mathrm{P}(\mathscr{T})}$ between the SE and MW bases, such that $\Psi_{\mathbf{i}}(\xi) = \sum_{\mathbf{j} \in SE^{\mathrm{No}}(\mathscr{T})} B_{\mathbf{ij}} \Phi_{\mathbf{j}}(\xi)$, for all $\mathbf{i} \in MW^{\mathrm{No}}(\mathscr{T})$, where $(B)_{\mathbf{ij}} = \left\langle \Psi_{\mathbf{i}} \Phi_{\mathbf{j}} \right\rangle$. The stochastic space $S^{\mathrm{No}}(\mathscr{T})$ with alternative SE or MW bases, namely $\{\Phi_{\mathbf{i}}\}_{\mathbf{i} \in SE^{\mathrm{No}}(\mathscr{T})}$ or $\{\Psi_{\mathbf{i}}\}_{\mathbf{i} \in MW^{\mathrm{No}}(\mathscr{T})}$, constitutes a discrete multiresolution approximation space.

General binary trees

The advantage of introducing complete binary trees is that the definitions of the SE and MW expansions remain unchanged when considering more general binary trees. Here, we consider binary trees with nodes having either two children or none. We

continue to denote by $\mathrm{Nr}(\mathscr{T})$ the maximum distance $|\mathtt{n}|$ over $\mathscr{N}(\mathscr{T})$, but we now allow $|\mathtt{l}| \leq \mathrm{Nr}(\mathscr{T})$ for some $\mathtt{l} \in \mathscr{L}(\mathscr{T})$. An example of incomplete binary tree is depicted in Figure 3.

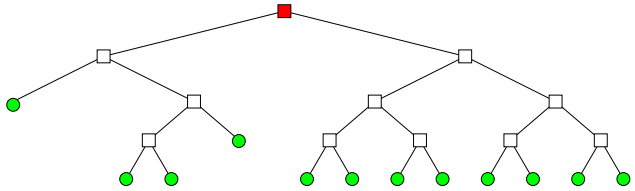

FIGURE 3. EXAMPLE OF INCOMPLETE BINARY TREE.

For such a tree $\mathscr{T}$, the SE and MW expansions of a random quantity $H(\xi)$ in (17) and (28) remain valid, together with their multi-index counterpart in (20) and (29) (upon redefining the multi-index sets $SE^{\mathrm{No}}(\mathscr{T})$ and $MW^{\mathrm{No}}(\mathscr{T})$). We also define $\mathrm{P}(\mathscr{T})$ according to (16). Consistently, we continue to denote by $S^{\mathrm{No}}(\mathscr{T})$ the stochastic approximation space associated with a tree $\mathscr{T}$, although it does not correspond to the full multiresolution space $S^{\mathrm{No}}(\mathscr{T}_{[\mathrm{Nr}]})$, but only to a subspace thereof, since the tree is incomplete. Finally, to alleviate the notation, we drop the superscript No since the developments below involve a fixed polynomial order.

We observe that, in addition to the summation over the P_π polynomial degrees of freedom, the SE expansion in (17) involves a summation over the set of leafs of the tree. In fact, if one needs to compute $H(\xi)$ for some ξ, the summation reduces to the unique leaf $\mathtt{l}$ such that $\xi \in S(\mathtt{l})$. As a result, the SE coefficients $h^{\mathtt{l}}_{1\leq\alpha\leq\mathrm{P}_\pi}$ of $H^{\mathscr{T}}$ are associated with the leaf $\mathtt{l}$. Conversely, the MW expansion in (28) consists of a summation over the full set of nodes except the leafs, which for given $\xi \in \Xi$ reduces to the set of ancestrors of the leaf $\mathtt{l}$ containing ξ. As a matter of fact, the multiwavelet coefficients $\tilde{h}^{\mathtt{l}}_{1\leq\alpha\leq\mathrm{P}_\pi}$ are associated with the nodes having descendants, with the special case of the root node yielding the coefficients $\tilde{h}^{\mathtt{n}_0}_{1\leq\alpha\leq\mathrm{P}_\pi}$. Finally, for later use, we define the following (partial order) inclusion relation between two trees $\mathscr{T}$ and $\mathscr{T}'$:

$$\mathscr{T} \subset \mathscr{T}' \iff \mathscr{N}(\mathscr{T}) \subset \mathscr{N}(\mathscr{T}'). \tag{30}$$

Multidimensional case

Consider now $\xi = (\xi_1, \ldots, \xi_{\mathrm{N}}) \in \Xi = [0,1]^{\mathrm{N}}$ with uniform joint density p_ξ. We simply extend the construction above for the case $\mathrm{N} = 1$ to the case $\mathrm{N} > 1$ by enriching the tree structure. Several possibilities can be considered. For instance, one can consider 2^{N}-ary tree structures (Quad-trees, Oct-tree, ...) but this approach is intrinsically limited to low dimension N. Here, we choose a different approach. First, we keep the binary structure of the tree (a node has none or two children) and introduce for each node $\mathtt{n} \in \mathscr{N}(\mathscr{T}) \setminus \mathscr{L}(\mathscr{T})$ an indicator, denoted by $\mathrm{d}(\mathtt{n}) \in \{1, \ldots, \mathrm{N}\}$, of the direction along which the dyadic partition is applied to construct its two children. For a leaf node $\mathtt{l}$ we conventionally set $\mathrm{d}(\mathtt{l}) = 0$. Second, the multidimensional polynomial basis $\{\Phi^{\mathtt{n}_0}_\alpha\}$ is constructed by tensorizations of one-dimensional normalized Legendre polynomials defined on $[0,1]$. The tensorization can be complete or partial; in any case, we denote by $\Pi^{\mathrm{N}}_{\mathrm{No}}$ the corresponding multidimensional polynomial space, and continue to denote by P_π its dimension. The approximation space defined in (15) then becomes

$$S(\mathscr{T}) = \{H : \Xi \to \mathbb{R}; \forall \mathtt{l} \in \mathscr{L}(\mathscr{T}), H|_{\mathscr{S}(\mathtt{l})} \in \Pi^{\mathrm{N}}_{\mathrm{No}}[\xi]\}, \tag{31}$$

whose dimension is still given by $SE(\mathscr{T}) = \mathrm{card}(\mathscr{L}(\mathscr{T})) \times \mathrm{P}_\pi$. Accordingly, the SE basis functions $\Phi^{\mathtt{n}}_\alpha(\xi)$ are defined using dimension-wise coordinate transformations, as in (18), leading to a SE expansion formally similar to (17). The extension of the MW basis is less straightforward because it is not possible to proceed by tensorization of the one-dimensional basis of $W^{\mathrm{No}}(\mathscr{T}_{[0]})$ to obtain a "universal" set of MW functions Ψ_α. This is due to the tree construction where to each node corresponds a partition along a unique direction $\mathrm{d}(\mathtt{n})$: the detail basis $\{\Psi^{\mathtt{n}}_\alpha\}$ associated with a node $\mathtt{n} \in \mathscr{N}(\mathscr{T}) \setminus \mathscr{L}(\mathscr{T})$ depends on $\mathrm{d}(\mathtt{n})$. However, there exist N sets of anisotropic detail functions $\{\Psi^{\mathrm{d}}\}_{1\leq\alpha\leq\mathrm{P}_\pi}$ that span the detail spaces supporting a partition in direction $1 \leq \mathrm{d} \leq \mathrm{N}$. For brevity, we do not discuss the construction of these functions here; we simply state the multidimensional MW expansion in the form

$$H^{\mathscr{T}}(\xi) = \sum_{\alpha=1}^{\mathrm{P}_\pi} h^{\mathtt{n}_0}_\alpha \Phi^{\mathtt{n}_0}_\alpha(\xi) + \sum_{\substack{\mathtt{n}\in\mathscr{N}(\mathscr{T}) \\ \mathtt{n}\notin\mathscr{L}(\mathscr{T})}} \left(\sum_{\alpha=1}^{\mathrm{P}_\pi} \tilde{h}^{\mathtt{n}}_\alpha \Psi^{\mathrm{d}(\mathtt{n}),\mathtt{n}}_\alpha(\xi) \right), \tag{32}$$

where $\Psi^{\mathrm{d}(\mathtt{n}),\mathtt{n}}_\alpha$ is a rescaled version of the anisotropic detail function associated with node $\mathtt{n}$. We observe that the expansion (32) can be recast into the generic form (29).

There is however an essential difference between one-dimensional and multidimensional binary trees: for $\mathrm{N} > 1$, there are in general more than one tree with the same set of leafs, *i.e.*, yielding the same partition of Ξ. This is illustrated in Figure 4 for $\mathrm{N} = 2$. Consequently, we say that two trees $\mathscr{T}$ and $\mathscr{T}'$ are equivalent if they share the same set of leafs,

$$\mathscr{T} \equiv \mathscr{T}' \Longleftrightarrow \mathscr{L}(\mathscr{T}) = \mathscr{L}(\mathscr{T}'). \tag{33}$$

Finally, the inclusion relation (30) is extended in the multidimensional case to

$$\mathscr{T} \subset \mathscr{T}' \Longleftrightarrow \exists \mathscr{T}'' \equiv \mathscr{T}',\ \mathscr{N}(\mathscr{T}) \subset \mathscr{N}(\mathscr{T}''). \tag{34}$$

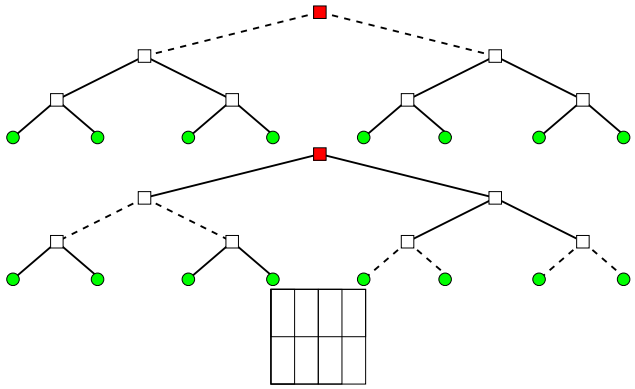

FIGURE 4. EXAMPLE FOR N = 2 OF TWO EQUIVALENT TREES LEADING TO THE SAME PARTITION OF Ξ (BOTTOM). THE SOLID (RESP. DASH) SEGMENTS REPRESENT A PARTITION ALONG THE FIRST (RESP. SECOND) DIRECTION.

ROE-TYPE SOLVER WITH ADAPTIVE STOCHASTIC DISCRETIZATION

We are interested in problems where a shock appears almost surely in finite time. Still, this shock remains localized both in the deterministic domain $\Omega \times [0,+\infty[$ for each realization of the parameters $\xi \in \Xi$, and in the uncertain parameter domain Ξ at a given point $(x,t) \in \Omega \times [0,+\infty[$. In other words, the solution is almost everywhere smooth on $\Omega \times [0,+\infty[\times \Xi$. This observation strongly advocates for the use of adaptive strategies where the computational effort is concentrated in the vicinity of shocks, while a coarser discretization is used where the solution is smooth. In what follows, we only consider adaptation of the stochastic discretization by relying on a fixed spatial mesh (the time-step satisfying a CFL condition to be specified later). However, we do seek for an adapted stochastic discretization that depends on the space variable x and the time t. In the context of the stochastic discretization framework introduced in the previous section, it amounts to an indexation with both x and t of the trees $\mathscr{T}$ defining the stochastic approximation space $S(\mathscr{T})$. Specifically, we now denote by $\mathscr{T}_i^n$ the tree associated with the i-th cell of the spatial mesh at the discrete time t^n, such that the approximate stochastic solution on the i-th cell at time t^n has for expansions

$$U_i^n(\xi) \approx (U_i^n)^{\mathscr{T}_i^n} = \sum_{\mathbf{j} \in SE(\mathscr{T}_i^n)} (u_i^n)_{\mathbf{j}} \Phi_{\mathbf{j}}(\xi) = \sum_{\mathbf{j} \in MW(\mathscr{T}_i^n)} (\widetilde{u_i^n})_{\mathbf{j}} \Psi_{\mathbf{j}}(\xi) \in S(\mathscr{T}_i^n). \quad (35)$$

We first extend the Roe-type solver to the tree formalism, while the adaptive procedure is discussed afterwards. To this purpose, we need to consider restriction and prediction operators between two different general binary trees. Such operations are described in detail in the next section. The restriction operation consists in restricting a quantity $H^{\mathscr{T}} \in S(\mathscr{T})$ to a smaller stochastic space $S(\mathscr{T}^-)$ where $\mathscr{T}^- \subset \mathscr{T}$. We denote by $\mathscr{R}_{\downarrow \mathscr{T}^-} H^{\mathscr{T}}$ this operator. The prediction operation consists in extending a quantity $H^{\mathscr{T}} \in S(\mathscr{T})$ on a larger stochastic space $S(\mathscr{T}^+)$ where $\mathscr{T} \subset \mathscr{T}^+$. We denote by $\mathscr{P}_{\uparrow \mathscr{T}^+} H^{\mathscr{T}}$ this operator.

Roe-type solver

The main ingredient of the Roe-type solver is the computation of the Galerkin Roe flux in (11). To fix the ideas, we focus on the determination of the flux $\varphi_{i-1/2} := \varphi^{\mathrm{Roe}}(u_L, u_R)$ from (11) at the interface $i-1/2$ between two neighboring cells $i-1$ and i, and where u_L and u_R denotes the vectors of expansion coefficients for the cells $i-1$ and i respectively.

Def nition of the left and right states. Because in general $\mathscr{T}_{i-1}^n \neq \mathscr{T}_i^n$, the vectors of expansion coefficients u_L and u_R are not defined with regard to the same stochastic basis functions, so that we first construct an intermediate tree $\mathscr{T}_{i-1/2}^n$ for the interface flux calculation which we define as the union of $\mathscr{T}_{i-1}^n$ and $\mathscr{T}_i^n$: for two generic trees $\mathscr{T}_1$ and $\mathscr{T}_2$ we define their union-tree $\mathscr{T}_{1\cup 2} := \mathscr{T}_1 \cup \mathscr{T}_2$ as (one of) the minimal tree(s) (in terms of number of leafs) such that for all $\mathtt{l} \in \mathscr{L}(\mathscr{T}_{1\cup 2})$,

$$\exists ! \mathtt{l}_1 \in \mathscr{L}(\mathscr{T}_1), \exists ! \mathtt{l}_2 \in \mathscr{L}(\mathscr{T}_2), \mathscr{S}(\mathtt{l}) = \mathscr{S}(\mathtt{l}_1) \cap \mathscr{S}(\mathtt{l}_2). \quad (36)$$

The union of two trees corresponding to two neighboring cells $i-1$ and i is illustrated in Figure 5 for N = 2. The union-tree is not unique whenever N > 1, as different minimal trees can be constructed to satisfy (36). These union-trees are all equivalent and yield the same stochastic space $S(\mathscr{T}_{1\cup 2})$. Moreover, it is readily verified that both $S(\mathscr{T}_1)$ and $S(\mathscr{T}_2)$ are subspaces of $S(\mathscr{T}_{1\cup 2})$. As a result, we can compute the left and right state SE expansion coefficients in $S(\mathscr{T}_{i-1/2})$ by means of the prediction operator: u_L and u_R are defined as the vector of SE coefficients on $S(\mathscr{T}_{i-1/2})$ of the predictions $\mathscr{P}_{\uparrow \mathscr{T}_{i-1/2}} (U_{i-1}^n)^{\mathscr{T}_{i-1}^n}$ and $\mathscr{P}_{\uparrow \mathscr{T}_{i-1/2}} (U_i^n)^{\mathscr{T}_i^n}$.

Roe f ux. At this point, we have to compute

$$\varphi_{i-1/2} = \frac{f(u_L) + f(u_R)}{2} - |a_{LR}^{\mathrm{Roe}}| \frac{u_R - u_L}{2}, \quad (37)$$

where the SE coefficients of the left and right states are defined on the same stochastic space $S(\mathscr{T}_{i-1/2})$. A key feature of the SE representation is that, owing to the orthogonality of the basis functions associated to distinct leafs (see (19)), it decouples

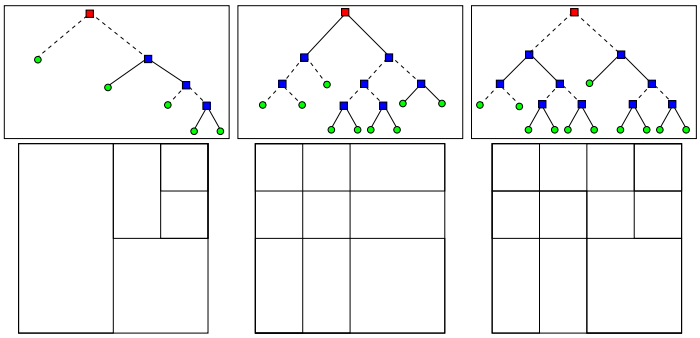

FIGURE 5. EXAMPLE FOR N = 2 OF THE UNION OF TWO TREES CORRESPONDING TO TWO NEIGHBORING CELLS $i-1$ AND i. TOP LINE: $\mathscr{T}_{i-1}^n$ (LEFT), $\mathscr{T}_i^n$ (CENTER), AND $\mathscr{T}_{i-1/2}$ (RIGHT). BOTTOM LINE: CORRESPONDING PARTITION OF THE PARAMETER SPACE. THE SOLID (RESP. DASH) SEGMENTS REPRESENT A PARTITION ALONG THE FIRST (RESP. SECOND) DIRECTION.

the flux computation over the set of leafs of the interface tree. Indeed, by defining the index set $SE(\mathscr{T}_{i-1/2})$ through consecutive enumeration of the coefficients related to a leaf, the matrix a_{LR}^{Roe} has a block diagonal structure. As a result, the Roe-type solver is applied independently on each leaf $\mathtt{l} \in \mathscr{L}(\mathscr{T}_{i-1/2})$, using the local basis $\{\Phi_1^{\mathtt{l}}, \ldots, \Phi_{\mathrm{P}_\pi}^{\mathtt{l}}\}$ in place of the generic basis $\{\Gamma_0, \ldots, \Gamma_{\mathrm{P}}\}$. In particular, denoting by $[a_{LR}^{\mathrm{Roe}}]_{\mathtt{l}}$ the $(m\mathrm{P}_\pi) \times (m\mathrm{P}_\pi)$ sub-matrix associated with the leaf $\mathtt{l} \in \mathscr{L}(\mathscr{T}_{i-1/2})$, we approximate its absolute value as follows:

$$\left|[a_{LR}^{\mathrm{Roe}}]_{\mathtt{l}}\right| \approx q_{d_{\mathrm{fit}},\{\lambda_1'\}}([a_{LR}^{\mathrm{Roe}}]_{\mathtt{l}}), \tag{38}$$

where $\{\lambda_1'\}$ is an approximate spectrum of $[a_{LR}^{\mathrm{Roe}}]_{\mathtt{l}}$ and $q_{d_{\mathrm{fit}},\{\lambda_1'\}}$ is the polynomial of degree $\leq d_{\mathrm{fit}}$ minimizing the quadratic functional

$$\sum_{\lambda \in \{\lambda_1'\}} \left(|\lambda| - q_{d_{\mathrm{fit}},\{\lambda_1'\}}(\lambda)\right)^2. \tag{39}$$

As in [7], we use for $\{\lambda_1'\}$ the set of eigenvalues of the original stochastic conservation law evaluated at the Gauss integration nodes over the leaf $\mathtt{l}$. Note that in the neighborhood of sonic points this Roe-type scheme requires a correction to obtain entropy solutions as detailed in [11].

Time integration. Since the fluxes have been computed for all the interfaces of the computational mesh, the remaining step is the time-integration of the solution according to (8). In general the fluxes $\varphi_{i-1/2}$ and $\varphi_{i+1/2}$ at the left and right interfaces as well as the current state u_i^n are defined over different trees. As for the flux computations, we construct $\mathscr{T}_i^{n+1} := \mathscr{T}_{i-1/2} \cup \mathscr{T}_{i+1/2}$ and remark that $\mathscr{T}_i^n \subset \mathscr{T}_i^{n+1}$. Therefore the left and right fluxes and the current state can be predicted on $\mathscr{T}_i^{n+1}$ before applying (8) to obtain u_i^{n+1} from the set of SE coefficients of $(U_i^{n+1})^{\mathscr{T}_i^n}$. To ensure the stability of the time-integration, the time step Δt^n has to be selected to satisfy the CFL condition in (12), where in the present adaptive context, the maximal characteristic velocity is taken over the full set of approximated spectra (for every leaf of every interface tree).

Adaptation

Starting from an initial data consisting, for each spatial cell, of a tree $\mathscr{T}_i^0$ and the corresponding approximation of the initial condition $U_i^0 \in S(\mathscr{T}_i^0)$, the above scheme refines the stochastic discretization, through the union operator, but in an uncontrolled fashion. Furthermore, all the trees eventually converge toward a unique tree which is the union of all the initial trees. Two additional ingredients are needed to obtain a fully adaptive method; first, an enrichment procedure where the trees are refined in a controlled way (in particular by allowing the generation of trees that are not included in $\cup_i \mathscr{T}_i^0$), and, second, a coarsening procedure to avoid the emergence of unnecessary complex trees for cells where the solution is smooth and can be accurately approximated on a low-dimensional stochastic space.

The heuristic ideas driving the enrichment and coarsening procedures are described in the next section. The enrichment procedure is applied when defining the trees for the flux evaluation. This choice can be motivated by observing that flux functions of interest are often nonlinear, so that approximation spaces larger than those for the solution are needed for accurate flux evaluation. For the coarsening procedure, it appears natural to analyze the solution at the end of the time step to decide whether details can be disregarded to save computational effort. With these choices, the adaptive algorithm over a time step takes the following form:

I) Loop over the interfaces: (**flux computation**)
   1. Define the enriched tree of the interface: $\mathscr{T}_{i-1/2} = \mathscr{E}\left(\mathscr{T}_{i-1}^n \cup \mathscr{T}_i^n\right)$
   2. Predict the left and right states on $S(\mathscr{T}_{i-1/2})$
   3. For each leaf $\mathtt{l} \in \mathscr{L}(\mathscr{T}_{i-1/2})$:
      (a) Compute the local fluxes $f_{\mathtt{l}}(u_L)$ and $f_{\mathtt{l}}(u_R)$ and the matrix $[a_{LR}^{\mathrm{Roe}}]_{\mathtt{l}}$
      (b) Determine the local polynomial $q_{d_{\mathrm{fit}},\{\lambda_1'\}}$
      (c) Assemble the contribution of the leaf to $\varphi_{i-1/2}$

II) Loop over the spatial cells: (**time integration**)
   1. Construct the cell integration tree: $\mathscr{T}_i^* = \mathscr{T}_{i-1/2} \cup \mathscr{T}_{i+1/2}$
   2. Predict the left / right fluxes and initial state on $S(\mathscr{T}_i^*)$
   3. Integrate to obtain $(U_i^*)^{\mathscr{T}_i^*}$

(**coarsening step**)

1. Coarsen the tree $\mathscr{T}_i^{n+1} = \mathscr{C}(\mathscr{T}_i^*) \subseteq \mathscr{T}_i^*$
2. Restrict the solution: $\left(U_i^{n+1}\right)^{\mathscr{T}_i^{n+1}} = \mathscr{R}_{\downarrow \mathscr{T}_i^{n+1}} \left(U_i^*\right)^{\mathscr{T}_i^*}$.

ALGORITHMIC ASPECTS

This section collects some details on the restriction and prediction operations, as well as on the enrichment and coarsening procedures.

Restriction operation. Given two general binary trees $\mathscr{T}^- \subset \mathscr{T}$ and given $H^{\mathscr{T}} \in S(\mathscr{T})$, we define the restriction $\mathscr{R}_{\downarrow \mathscr{T}^-} H^{\mathscr{T}}$ of $H^{\mathscr{T}}$ to $S(\mathscr{T}^-)$ as the orthogonal $L^2(\Xi, p_\xi)$-projection of $H^{\mathscr{T}}$ on $S(\mathscr{T}^-)$ (observe that by construction, $S(\mathscr{T}^-) \subset S(\mathscr{T})$), that is,

$$\left\langle \left(H^{\mathscr{T}} - \mathscr{R}_{\downarrow \mathscr{T}^-} H^{\mathscr{T}} \right) \Phi \right\rangle = 0, \quad \forall \Phi \in S(\mathscr{T}^-). \tag{40}$$

In terms of multiwavelet coefficients, the restriction operation is straightforward. Letting $\tilde{h}^{\mathtt{n}}_\alpha$ be the MW coefficients of $H^{\mathscr{T}}$, we obtain for all $1 \le \alpha \le \mathrm{P}_\pi$,

$$\left(\widetilde{\mathscr{R}_{\downarrow \mathscr{T}^-} H^{\mathscr{T}}} \right)^{\mathtt{n}}_\alpha = \tilde{h}^{\mathtt{n}}_\alpha, \ \forall \mathtt{n} \in \mathscr{N}(\mathscr{T}^-) \setminus \mathscr{L}(\mathscr{T}^-). \tag{41}$$

Computation of the SE coefficients of the restriction is not as immediate as for the MW coefficients. One possibility is to rely on the expressions (41) together with the transition matrix B to obtain the SE coefficients $\left(\mathscr{R}_{\downarrow \mathscr{T}^-} H^{\mathscr{T}}\right)^{\mathtt{n}}_\alpha$. However, assembly of $B(\mathscr{T}^-)$ (or directely of its inverse) can be quite expensive for stochastic spaces with large dimension, and it appears more efficient in practice to proceed recursively. Assuming that the SE expansion of $H^{\mathscr{T}}$ is known, we construct a sequence of trees $\mathscr{T}^{(i)}$ such that

$$\mathscr{T} = \mathscr{T}^{(0)} \supset \mathscr{T}^{(1)} \supset \cdots \supset \mathscr{T}^{(i)} \supset \cdots \supset \mathscr{T}^{(l)} = \mathscr{T}^-, \tag{42}$$

where two consecutive trees differ by one generation only, *i.e.* a leaf of $\mathscr{T}^{(i+1)}$ is either a leaf or a node with leaf children in $\mathscr{T}^{(i)}$. Therefore the transition from $\mathscr{T}^{(i)}$ to $\mathscr{T}^{(i+1)}$ consists in removing a set of pairs of sister leafs to reduce iteratively the tree. The process is illustrated in Figure 6 in the case of the reduction of a unique pair of leafs. Focusing on the removal of a (left-right ordered) pair of sister leafs $\{\mathtt{l}^-, \mathtt{l}^+\} \in \mathscr{L}(\mathscr{T}^{(i)})$, the SE coefficients of the restriction of $H^{\mathscr{T}^{(i)}}$ associated with the leaf $\mathtt{l} = \mathtt{p}(\mathtt{l}^-) = \mathtt{p}(\mathtt{l}^+) \in \mathscr{L}(\mathscr{T}^{(i+1)})$ can be expressed in the

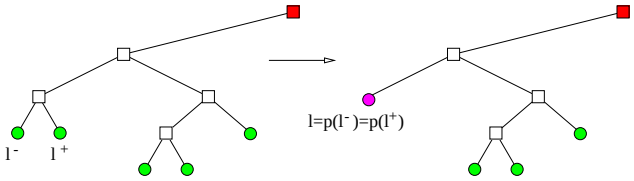

FIGURE 6. EXAMPLE OF TREE RESTRICTION THROUGH THE REMOVAL OF THE TWO CHILDREN LEAFS OF A NODE. ONLY PART OF THE TREES ARE SHOWN FOR CLARITY.

one-dimensional case $\mathrm{N} = 1$ as

$$h^{\mathtt{l}}_\alpha = \sum_{\beta=1}^{\mathrm{P}_\pi} \left[R^-_{\alpha,\beta} h^{\mathtt{l}^-}_\beta + R^+_{\alpha,\beta} h^{\mathtt{l}^+}_\beta \right], \tag{43}$$

where the transition coefficients of the linear combination are given by

$$R^-_{\alpha,\beta} = \left\langle \Phi^{\mathtt{l}}_\alpha \Phi^{\mathtt{l}^-}_\beta \right\rangle \text{ and } R^+_{\alpha,\beta} = \left\langle \Phi^{\mathtt{l}}_\alpha \Phi^{\mathtt{l}^+}_\beta \right\rangle. \tag{44}$$

In fact, the transition coefficients $R^-_{\alpha,\beta}$ and $R^+_{\alpha,\beta}$ are support and scale invariant (independent of $|\mathtt{l}|$ and $\mathscr{S}(\mathtt{l})$). For instance, in the simplest case $\mathrm{No} = 0$ ($\mathrm{P}_\pi = 1$), we have $R^-_{1,1} = R^+_{1,1} = 1/\sqrt{2}$. In the multi-dimensional case $\mathrm{N} > 1$, the prediction operator can be expressed using a family of N matrices $R^{\pm,\mathrm{d}}$ for $1 \le \mathrm{d} \le \mathrm{N}$.

Prediction operator. Given two general binary trees $\mathscr{T} \subset \mathscr{T}^+$ and given $H^{\mathscr{T}} \in S(\mathscr{T})$, there are several ways to define the prediction $\mathscr{P}_{\uparrow \mathscr{T}^+} H^{\mathscr{T}}$ of $H^{\mathscr{T}}$ on $S(\mathscr{T}^+)$; see *e.g.* [12,13]. Here we consider a simple approach, where no information is generated by the prediction. As for the restriction operation, the MW expansion of the prediction is immediately inferred from the MW expansion coefficients of $H^{\mathscr{T}}$ in $S(\mathscr{T})$. We obtain for all $1 \le \alpha \le \mathrm{P}_\pi$ and $\mathtt{n} \in \mathscr{N}(\mathscr{T}^+) \setminus \mathscr{L}(\mathscr{T}^+)$,

$$\left(\widetilde{\mathscr{P}_{\uparrow \mathscr{T}^+} H^{\mathscr{T}}} \right)^{\mathtt{n}}_\alpha = \begin{cases} \tilde{h}^{\mathtt{n}}_\alpha, & \mathtt{n} \in \mathscr{N}(\mathscr{T}) \setminus \mathscr{L}(\mathscr{T}), \\ 0, & \text{otherwise.} \end{cases} \tag{45}$$

For the SE expansion coefficients of the prediction, we can again proceed iteratively using a series of increasing intermediate trees, differing by only one generation from one to the other. This time, the elementary operation consists in adding children to some leaf of the current tree, as illustrated in Figure 7. The SE coefficients associated to the new leafs can be expressed in the one-dimensional case $\mathrm{N} = 1$ as

$$h^{\mathtt{c}^-(\mathtt{n})}_\alpha = \sum_{\beta=1}^{\mathrm{P}_\pi} R^-_{\alpha,\beta} h^{\mathtt{n}}_\beta, \quad h^{\mathtt{c}^+(\mathtt{n})}_\alpha = \sum_{\beta=1}^{\mathrm{P}_\pi} R^+_{\alpha,\beta} h^{\mathtt{n}}_\beta, \tag{46}$$

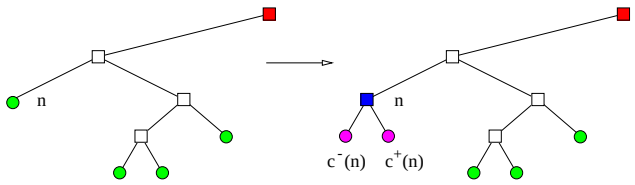

FIGURE 7. EXAMPLE OF EXTENSION OF A TREE THROUGH THE CREATION OF THE CHILDREN OF A LEAD NODE. ONLY PART OF THE TREES ARE SHOWN FOR CLARITY.

with the transition coefficients given by (44). As before, the family of N matrices $R^{\pm,\mathrm{d}}$ for $1 \le \mathrm{d} \le \mathrm{N}$ is considered in the multi-dimensional case $\mathrm{N} > 1$.

Finally, for two trees $\mathscr{T} \subset \mathscr{T}^+$, we observe that $\mathscr{R}_{\downarrow\mathscr{T}} \circ \mathscr{P}_{\uparrow\mathscr{T}^+} = Id_{S(\mathscr{T})}$, while in general $\mathscr{P}_{\uparrow\mathscr{T}^+} \circ \mathscr{R}_{\downarrow\mathscr{T}} \neq Id_{S(\mathscr{T}^+)}$.

Enrichment procedure. The purpose of the enrichment procedure is to compute the interface flux in a stochastic space larger than $S(\mathscr{T}_{i-1}^n \cup \mathscr{T}_i^n)$. It amounts to an extension of the union tree, by subdividing some of its leafs. Different strategies can be used. For instance, we can use the multiwavelet coefficients of the predictions of the left and right states to decide where to refine the tree as done for instance in [9, 15]. In this work and for the examples below, we simply decided to enrich the tree by splitting all the leafs of the union tree $\mathscr{T}_{i-1}^n \cup \mathscr{T}_i^n$ along each of the N directions of the stochastic parameter domain. In doing so, the enriched tree $\mathscr{T}_{i-1/2} = \mathscr{E}(\mathscr{T}_{i-1}^n \cup \mathscr{T}_i^n)$ has a total of $(2^{\mathrm{N}})card(\mathscr{L}(\mathscr{T}_{i-1}^n \cup \mathscr{T}_i^n))$ leafs, showing that such a straightforward enrichment is only practical in situations where N is small: it will be necessary to consider more advanced strategies in the future.

Coarsening procedure. The coarsening procedure is applied after the time integration, when the solution for the i-th cell is known on a tree $\mathscr{T}_i^*$. The objective is to define a subtree $\mathscr{T}_i^{n+1} \subseteq \mathscr{T}_i^*$ so that the dimension of $S(\mathscr{T}_i^{n+1})$ is reduced while the restriction error $U^{\mathscr{T}_i^*} - \mathscr{R}_{\downarrow\mathscr{T}_i^{n+1}} U^{\mathscr{T}_i^*}$ remains acceptable. In wavelet methods, one usually defines the coarsening through a thresholding procedure in which wavelet coefficients with absolute value less than a prescribed threshold value are disregarded. This concept can be extended to the multiwavelet discretization too. However, we need to introduce some constraints in order to maintain a binary tree structure for the resulting tree. Specifically, we construct a sequence of imbricated trees, obtained through the removal of pairs of sister-leafs from one tree to the next. For a couple of sister-leafs having node $\mathtt{n}$ for parent, we remove the two leafs if

$$\sum_{\alpha=1}^{\mathrm{P}_\pi} (\tilde{u}_\alpha^{\mathtt{n}})^2 < \varepsilon_c^2, \tag{47}$$

where $\varepsilon_c > 0$ is the threshold parameter that may be a function of the depth $|\mathtt{n}|$ of the parent node. The criterion (47) is heuristic and based on the $L_2(\Xi, p_\xi)$ stochastic norm of the MW details associated with the parent node $\mathtt{n}$. The coarsening sequence is stopped whenever no couple of sister-leafs can be removed.

We remark that this algorithm only generates trees consistent with $\mathscr{T}_i^*$ in the sense that, along the sequence, the successive (coarser and coarser) partitions of Ξ follow, in backward order, the nodes' partition direction $\mathrm{d}(\mathtt{n})$ as prescribed by $\mathscr{T}_i^*$. (Recall that the multiwavelet basis, and so the MW coefficients, depend on the partition directions $\mathrm{d}(\mathtt{n})$.) In other words, the coarsening can only "undo" partitions following the structure imposed by $\mathscr{T}_i^*$. This is clearly unsatisfying because for $\mathrm{N} > 1$, there are multiple trees equivalent to $\mathscr{T}_i^*$ and we would like the coarsened tree to be independent of any particular choice for $\mathscr{T}_i^*$. To avoid arbitrariness, the trees of the sequence are periodically substituted by an equivalent one. These equivalent trees are constructed by searching in the current tree structures the pattern of a node $\mathtt{n}$ whose children $\mathtt{c}^-(\mathtt{n})$ and $\mathtt{c}^+(\mathtt{n})$ are subsequently partitioned along a same direction: $\mathrm{d}(\mathtt{c}^+(\mathtt{n})) = \mathrm{d}(\mathtt{c}^-(\mathtt{n})) \neq 0$. When such a pattern is found, partition directions are exchanged, $\mathrm{d}(\mathtt{n}) \leftrightarrow \mathrm{d}(\mathtt{c}^-(\mathtt{n})) = \mathrm{d}(\mathtt{c}^+(\mathtt{n}))$, together with a permutation of the descendants of the children nodes. This operation, illustrated in Figure 8, is applied periodically and randomly in the coarsening procedure.

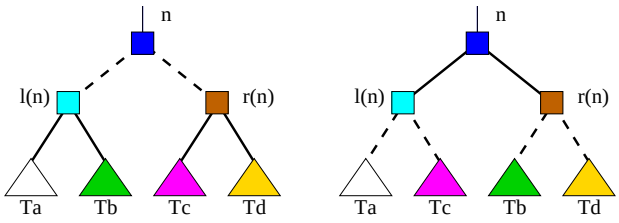

FIGURE 8. ILLUSTRATION OF THE ELEMENTARY OPERATION TO GENERATE EQUIVALENT TREES: THE PATTERN, OF A NODE WITH ITS TWO CHILDREN DIVIDED ALONG THE SAME DIRECTION, (LEFT GRAPH) IS REPLACED BY THE SAME PATTERN BUT WITH THE PARTITION DIRECTIONS EXCHANGED (RIGHT GRAPH) PLUS A PERMUTATION OF THE SUBS-TREES (TRIANGLES) OF THE CHILDREN'S DESCENDENTS.

RESULTS

The proposed method is assessed on the Burgers equation with uncertain initial conditions and two stochastic dimensions. The basis at the SE level considered here corresponds to fully tensorized Legendre polynomials with degree $\le$ No.

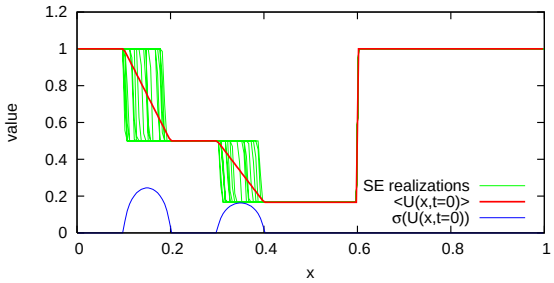

FIGURE 9. RANDOM INITIAL CONDITION FOR TEST CASE 1: SAMPLE SET OF 20 RANDOM REALIZATIONS, MEAN AND STANDARD DEVIATION.

Shocks with deterministic velocities

We consider a one-dimensional spatial domain $\Omega = [0,1]$ with periodic boundary conditions. The governing equation, in conservative form, is

$$\frac{\partial U}{\partial t} + \frac{\partial F(U)}{\partial x} = 0, \quad F(U) = \frac{U^2}{2}, \tag{48}$$

and we consider an uncertain initial condition $U^0(x,\xi)$ consisting of three piecewise constant deterministic states in x. Specifically, the three states are $\bar{u}^1 = 1$, $\bar{u}^2 = 1/2$, and $\bar{u}^3 = 1/6$, and the position of some jumps is uncertain: the jump from states $\bar{u}^1$ to $\bar{u}^2$ occurs at a random location $X_{1,2}$ having a uniform distribution in $[0.1, 0.2]$, while the jump from states $\bar{u}^2$ to $\bar{u}^3$ occurs at a random location $X_{2,3}$ having a uniform distribution in $[0.3, 0.4]$. Finally, the jump from states $\bar{u}^3$ to $\bar{u}^1$ is at $x_{31} = 0.6$. The random locations $X_{1,2}$ and $X_{2,3}$ are independent and parameterized using two independent random variables ξ_1 and ξ_2 respectively, both with uniform distribution in $[0,1]$:

$$X_{1,2} = 0.1 + 0.1\xi_1, \quad X_{2,3} = 0.3 + 0.1\xi_2, \quad \xi_1, \xi_2 \sim \mathscr{U}[0,1]. \tag{49}$$

Therefore, the problem has two stochastic dimensions (N = 2). For this experiment, we constrained the trees so that the minimum depth level $|\mathfrak{n}|$ is 1 for all nodes and use a coarsening parameter $\varepsilon_c = 10^{-4}$. The polynomial order is No = 3. In Figure 9, we illustrate the random initial condition for a spatial discretization with Nc = 200 uniform cells in the spatial domain. The plot shows a sample set of 20 realizations of the random initial condition, together with its expectation and standard deviation.

In Figure 10 we show the stochastic solution at times $t = 0.2$ and 0.6. The solution expectation and standard deviation, together with a random sample set of realizations, are also plotted. The realizations are reconstructed from the stochastic expansions of the solutions, using a unique set of randomly generated realizations of $\xi \in \Xi = [0,1]^2$. For $t = 0.2$, the first shock whose velocity is $3/4$ has not yet reached the second shock whose velocity is $1/3$. At $t = 0.6$, the shocks have merged for nearly all realizations. Furthermore, the space-time diagrams of the solution expectation and standard deviation are plotted over the period of time $t \in [0,2]$ in Figure 11. We observe that the proposed adaptive method correctly captures the dynamics of the Burgers equation. The shocks are transported with the correct deterministic velocities and spurious uncertainty in the solution is not created. The stochastic resolution is adapted in space and time to the local smoothness of the solution in the stochastic domain such that we expect a finer stochastic discretization along the path of the shock waves depending on the variability in the solution. This is illustrated in Figure 12, where the stochastic solution $U(x_o(t),t,\xi)$ is plotted as a function of (ξ_1,ξ_2) for various times $t \in [0.2, 0.6]$ at a moving observation point $x_o(t) = 0.25 + 0.5t$ initially located between the two shocks. Since x_o moves slower than the first shock, x_o is eventually caught-up by the first random shock. Moreover, since x_o moves faster than the second shock, there is a time interval for which the stochastic solution at x_o corresponds to a set of events ξ with different configurations of the shocks. For $t = 0.2$, the observation point starts to be caught-up by some events corresponding to the largest realizations of $X_{1,2}$: the solution is a function of ξ_1 only. Hence we observe that the stochastic domain is more finely refined in the ξ_1-direction. At $t = 0.4$, the observation point starts to reach the second shock, introducing some dependence on ξ_2, while a fraction of events corresponds to shocks having merged. This creates a stochastic solution with three distinct plateaus with respective values 1, $1/2$, and $1/6$, whose configuration evolves in time. We obtain as expected a local adaptation of the stochastic discretization depending on spa-

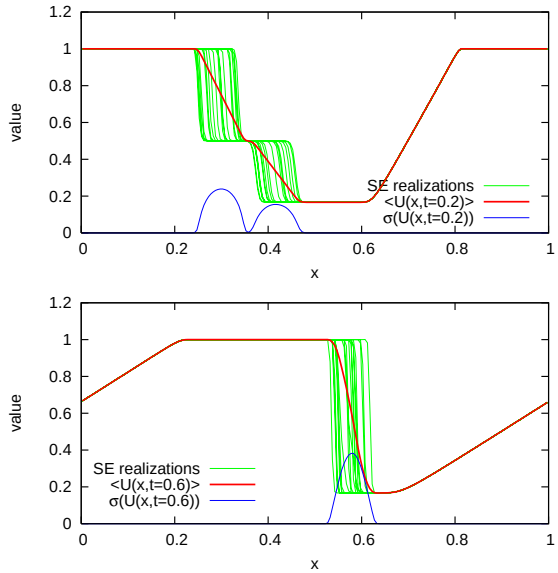

FIGURE 10. SOLUTION OF THE STOCHASTIC BURGERS EQUATION AT $t = 0.2$ AND $t = 0.6$. SAMPLE SET OF 20 RANDOM REALIZATIONS, MEAN AND STANDARD DEVIATION.

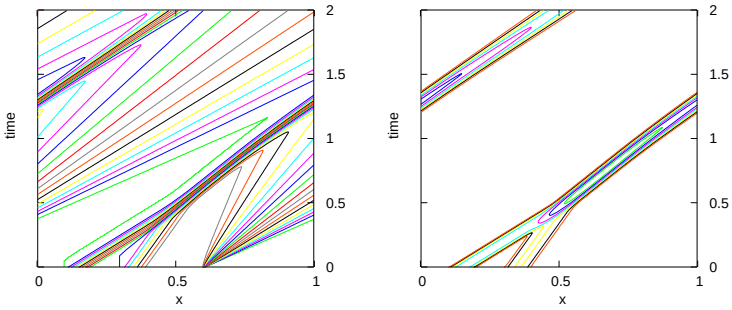

FIGURE 11. SPACE-TIME DIAGRAMS OF THE EXPECTATION (LEFT) AND STANDARD DEVIATION (RIGHT) OF THE STOCHASTIC BURGERS EQUATION.

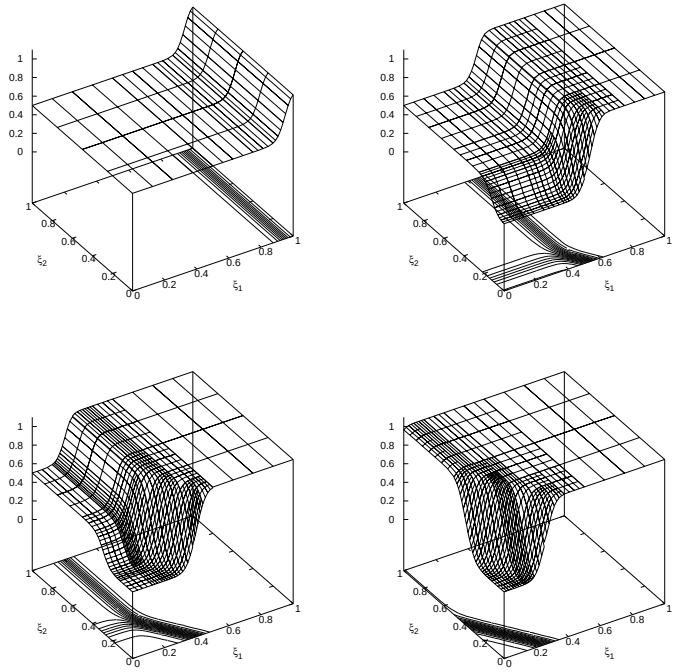

FIGURE 12. SOLUTION IN THE STOCHASTIC DOMAIN $(\xi_1,\xi_2)\in[0,1]^2$ FOR A MOVING POINT $x_o(t)=0.25+0.5t$ FOR DIFFERENT TIMES $t=0.2,0.4,0.5,0.6$.

tial position and time; the stochastic domain is finely discretized in the neighborhood of the discontinuities (in fact of the steep parts because of the diffusivity of the Roe scheme), while it is coarsely refined elsewhere.

Shocks with uncertain velocities

We still consider the Burgers equation, but with stochastic initial condition $U^0(x,\xi)$ defined using two uncertain states, $U^+(\xi_1)$ and $U^-(\xi_2)$, the first one almost surely positive and the second one almost surely negative. We take for $x\in[0,1]$,

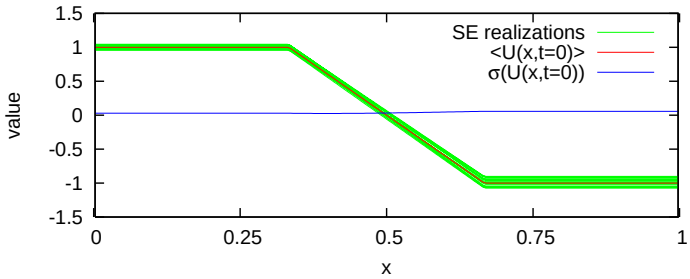

FIGURE 13. RANDOM INITIAL CONDITION OF THE STOCHASTIC BURGERS EQUATION FOR TEST CASE 2: SAMPLE SET OF 20 RANDOM REALIZATIONS, MEAN AND STANDARD DEVIATION.

$$U^0(x,\xi)=\begin{cases}U^+(\xi_1) & x<1/3,\\ U^-(\xi_2) & x>2/3,\\ U^+(\xi_1)(2-3x)+U^-(\xi_2)(3x-1) & 1/3\le x\le 2/3,\end{cases} \tag{50}$$

such that $U^0(x,\xi)$ is continuous for any $\xi\in[0,1]^2$. We define the stochastic states as

$$\begin{aligned} U^+(\xi_1)&=1-0.05(2\xi_1-1), && \xi_1\sim\mathscr{U}[0,1],\\ U^-(\xi_2)&=-1-0.1(2\xi_2-1), && \xi_2\sim\mathscr{U}[0,1], \end{aligned} \tag{51}$$

so that $U^+\sim\mathscr{U}[0.95,1.05]$ and $U^-\sim\mathscr{U}[-1.1,-0.9]$. We solve the stochastic Burgers equation with Dirichlet boundary conditions, $U=U^+$ at $x=0$ and $U=U^-$ at $x=1$. The initial condition is illustrated in Figure 13. $\mathrm{Nc}=201$ cells are used for space discretization.

Although initially continuous, the stochastic solution develops in finite time a discontinuity with a stochastic jump $|U^+-U^-|$ and a stochastic propagation velocity $(U^++U^-)/2$. The stochastic character of the shock magnitude and velocity has to be contrasted with the situation of the previous test case, where the jumps and shock velocity were certain.

To illustrate the refinement procedure, we present in Figure 14 the resulting partition of the parameter space Ξ at three different locations in space close to the center of the computational domain, $x=0.5\pm0.02$, and times $t=0.2,\ 0.4$, and 1.5. For this experiment, we constrained the trees so that $2\le|\mathfrak{n}|\le 12$ for all nodes and used a coarsening parameter $\varepsilon_c=10^{-4}$. The polynomial order is $\mathrm{No}=1$. The solution at the same times and over the part of the computational domain $x\in[0.35,0.65]$ is shown in Figure 15, where the solution expectation and standard deviation, together with a random sample set of realizations, are also plotted. The vertical red lines in Figure 15 indicate the

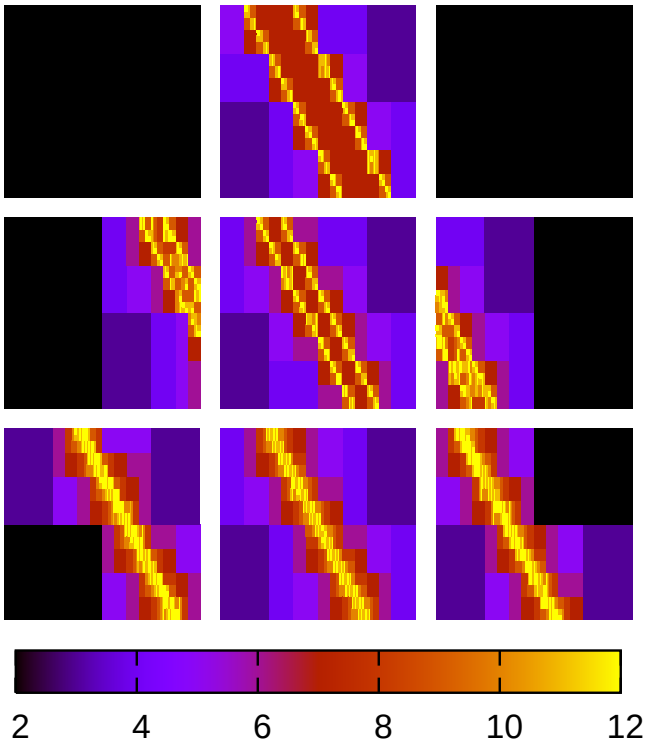

FIGURE 14. PARTITION OF THE PARAMETER SPACE Ξ AT TIMES 0.2, 0.4 AND 1.5 (FROM TOP TO BOTTOM) AND SPATIAL LOCATIONS $x = 0.48$, 0.5 AND 0.52 (FROM LEFT TO RIGHT). THE COLOR SCALE GIVES THE DEPTH OF THE LEAFS.

positions in space ($x = 0.5 \pm 0.02$) for which the partition of the parameter space is shown in Figure 14.

Figures 14 and 15 deserve some comments. At $t = 0.2$, the trees at $x = 0.5 \pm 0.02$ are such that $\mathrm{Nr}(\mathscr{T}) = 2$, the minimal value, since there the solution is still smooth in the stochastic domain at that time and spatial position. For $x = 0.5$, stochastic details are necessary to capture the shock who has formed almost surely and the maximum depth level $|\mathtt{n}|_{\max}$ for the trees has been already reached along two distinct lines across Ξ. In between these two lines, we observe that the maximum depth level is not reached. This region corresponds to a portion of the parameter space Ξ where the solution is smooth because of the diffusivity of the Roe scheme. This is reflected in the stochastic solution $U(\xi_1, \xi_2)$ at $x = 0.5$ and $t = 0.2$ in the left panel of Figure 16, where intermediate states $U^- < U(\xi) < U^+$ are seen. As time increases, the distance between the two lines corresponding to maximum refinement decreases, reflecting a steeper and steeper stochastic solution with regard to ξ (see plots for $t = 0.4$ and $t = 1.5$ in Figure 14 and the right panel of Figure 16). Due to the shock velocity $(U^+ + U^-)/2$, the shock has reached locations $x = 0.5 \pm 0.02$ with a probability contained in $]0,1[$, so that details are now needed over a portion of Ξ to account for the solution

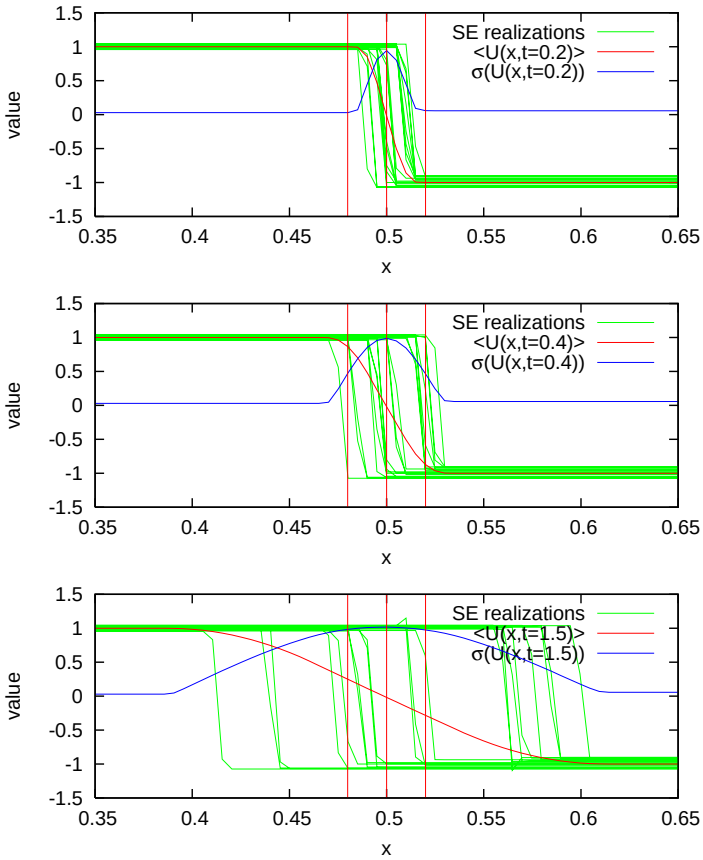

FIGURE 15. STOCHASTIC SOLUTION AT TIMES $t = 0.2$, 0.4 AND 1.5 (FROM TOP TO BOTTOM). SAMPLE SET OF 20 RANDOM REALIZATIONS, MEAN AND STANDARD DEVIATION. NUMERICAL PARAMETERS ARE GIVEN IN THE TEXT. ONLY A PART OF THE DOMAIN IS SHOWN FOR CLARITY.

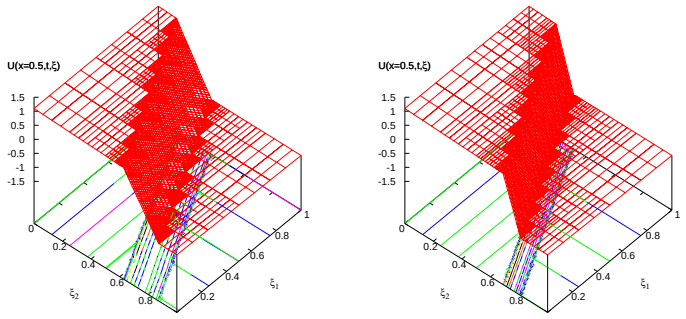

FIGURE 16. STOCHASTIC SOLUTION OF THE BURGERS EQUATION AS A FUNCTION OF (ξ_1, ξ_2) AT $x_o = 0.5$ AND $t = 0.2$ (LEFT) AND $t = 0.4$ (RIGHT).

discontinuity; in fact, details are needed only over half of the stochastic parameter domain at these two locations and time. We observe a drift of the shock location in the parameter domain at $x = 0.5 \pm 0.02$ between $t = 0.4$ and $t = 1.5$. This is due to the fact that the initial condition is almost surely non-symmetric, so that some realizations of the shocks will propagate to the left of the domain and some other to the right. Moreover, we expect that for a time large enough, we have at any spatial location a partition of the parameter space Ξ similar to the partition at $x = 0.5$ for $t = 1.5$, and a shocked stochastic solution with states U^+ or U^- according to the sign of $2(\xi_1 - 1/2) + (\xi_2 - 1/2)$ since the shock velocity is $(U^+ + U^-)/2$. This is reflected on the bottom line of Figure 14.

One of the important features of the adaptive strategy is that the refinement controls the magnitude and probability measure of the overshoots in the stochastic solution created by the discontinuities. To illustrate this assertion, we repeat the previous experiment, varying the maximum depth level allowed and compare solutions at $t = 1.5$. In Figure 17, we indeed observe a decay of the occurrence and magnitude of the overshoots when we increase the allowed maximal depth of the trees. Figure 18 presents the time evolution of the total number of leafs in the discrete solution, for various maximal depths, and below, the distribution of the leafs in space and time (note the vertical log scale) for the case $|\mathtt{n}| \leq 14$. For early times $t \lesssim 0.15$, the number of leafs is essentially independent of $|\mathtt{n}|_{\max}$, since the shock has not formed yet so that the adaptation is controlled by ε_c. At later times, the number of leafs increases roughly linearly with t, reflecting the linear dependence on t of the portion of Ω affected by the stochastic shock as seen from the bottom plot of Figure 18. Interestingly, when $|\mathtt{n}|_{\max}$ is increased by 2, the number of leafs is multiplied by less than 4.

To analyze the efficiency of the proposed adaptive methodology, we compare it with the corresponding method using a uniform discretization of the stochastic domain, that is, using fixed resolution level Nr (*i.e.* fixed depth of tree $\mathrm{Nr}(\mathscr{T})$ in each spatial cell). Figure 19 presents a random sample set of 30 realizations of the stochastic solution at $t = 1.5$ obtained with uniform resolution level $\mathrm{Nr} = 3$ and 4. The uniform resolution levels $\mathrm{Nr} = 3$ and 4 have been chosen in such a way that the total number of degrees of freedom in the uniform case, that is, $\mathrm{dof}_{\mathrm{unif}} = \mathrm{P}(\mathscr{T}_{[\mathrm{Nr}]}) \times \mathrm{Nc}$, is of the same order of magnitude as the total number of degrees of freedom in the adaptive case at $t^n = 1.5$, that is, $\mathrm{dof}_{\mathrm{adap}} = \sum_{\mathrm{i}=1}^{\mathrm{Nc}} \mathrm{P}(\mathscr{T}_{\mathrm{i}}^{\mathtt{n}})$. Thus, these results are to be compared with the panels of the second line of Figure 17 for maximum depth of the adaptive trees $|\mathtt{n}|_{\max} = 12$ and 14. We observe that the occurence and the magnitude of the overshoots is considerably reduced when using the adaptive method.

To evaluate more quantatively the control of overshoots, we measure the magnitude of overshoots integrated on the spatial

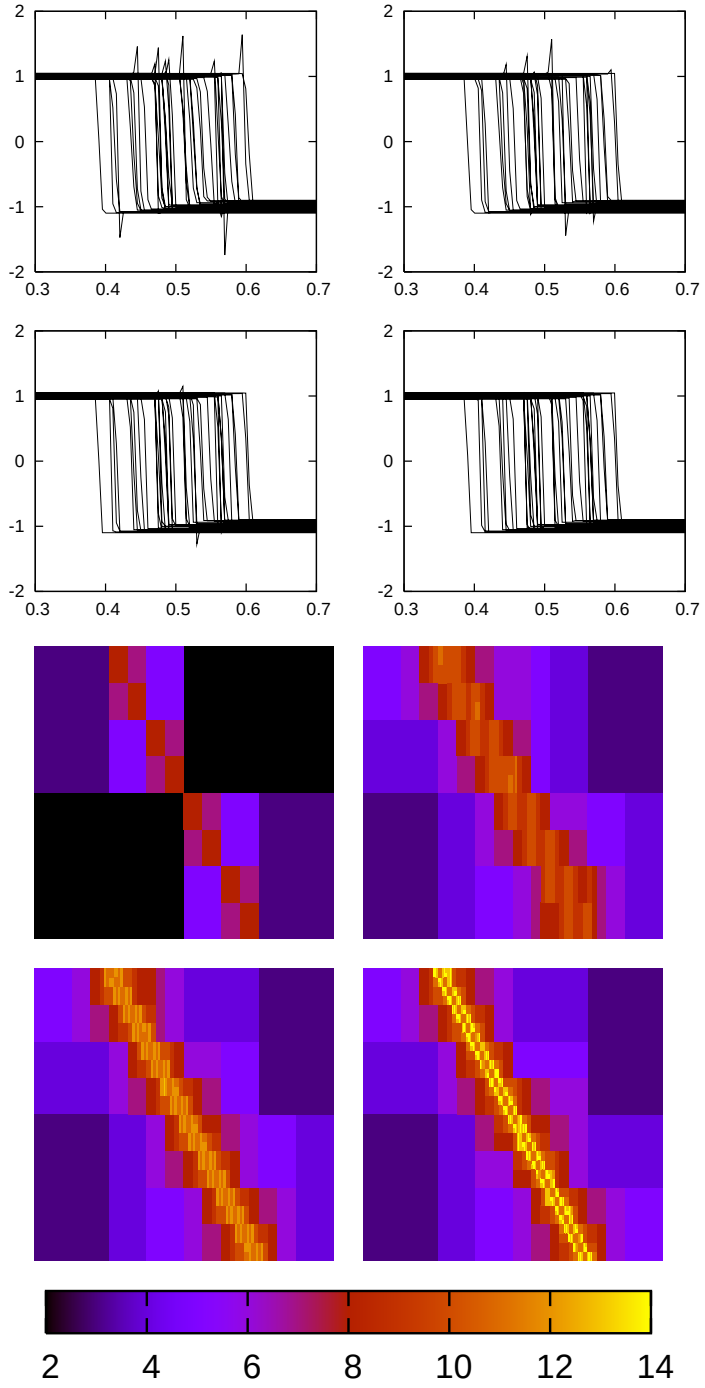

FIGURE 17. SAMPLE SET OF 30 REALIZATIONS OF THE COMPUTED STOCHASTIC SOLUTION AT $t = 1.5$, FOR MAXIMUM DEPTH OF THE TREES EQUAL TO 8 (TL), 10 (TR), 12 (BL) AND 14 (BR), AND CORRESPONDING STOCHASTIC MESHES AT $x = 0.5$. OTHER NUMERICAL PARAMETERS ARE GIVEN IN THE TEXT.

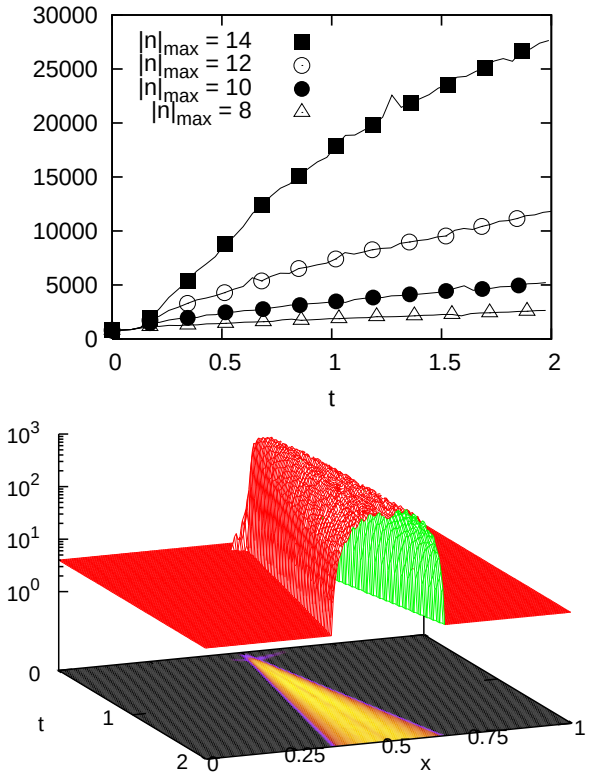

FIGURE 18. TOP: EVOLUTION WITH TIME OF TOTAL NUMBER OF LEAFS FOR THE APPROXIMATE SOLUTIONS USING MAXIMUM DEPTH LEVELS 8, 10, 12 AND 14. BOTTOM: SPACE-TIME DISTRIBUTION OF THE NUMBER OF LEAFS FOR THE TREES OF THE APPROXIMATE SOLUTION USING A MAXIMUM DEPTH LEVEL EQUAL TO 14.

domain as follows:

$$\varepsilon^2_{\text{over}}(t^n = 1.5) = \frac{\Delta x}{M} \sum_{i=1}^{\text{Nc}} \sum_{j=1}^{M} \Big((U_i^n(\xi^{(j)}) - U^+(\xi^{(j)}))_+^2 + (U_i^n(\xi^{(j)}) - U^-(\xi^{(j)}))_-^2 \Big), \quad (52)$$

where $U_i^n(\xi^{(j)})$ denotes the discrete stochastic solution evaluated at $\xi^{(j)}$ belonging to a random sample set, $U^{\pm}(\xi^{(j)})$ denote the exact upper and lower bounds on the stochastic solution at $\xi^{(j)}$, and the subscripts $_\pm$ denote the positive and negative part of a real number. We use a sample set with cardinality $M = 10^6$. Figure 20 presents the quantity $\varepsilon_{\text{over}}$ as a function of degrees of freedom (note the log scales) for $\text{Nr} = 1,2,3,4,5,6$ and $|\mathfrak{n}|_{\max} = 4,6,8,10,12,14$. Since the number of degrees of freedom for the adaptive method depends on time, we used conventionally the mean number of degrees of freedom in the time interval $[0,1.5]$. We observe that $\varepsilon_{\text{over}}$ decreases faster for the

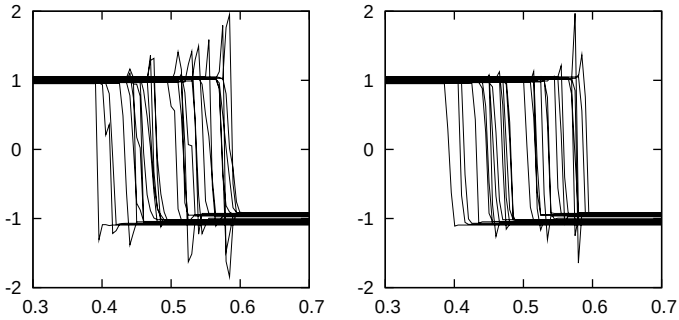

FIGURE 19. SAMPLE SET OF 30 REALIZATIONS OF THE COMPUTED STOCHASTIC SOLUTION AT $t = 1.5$, IN THE CASE OF A UNIFORM DISCRETIZATION OF THE STOCHASTIC DOMAIN FOR RESOLUTION LEVEL Nr EQUAL TO 3 AND 4.

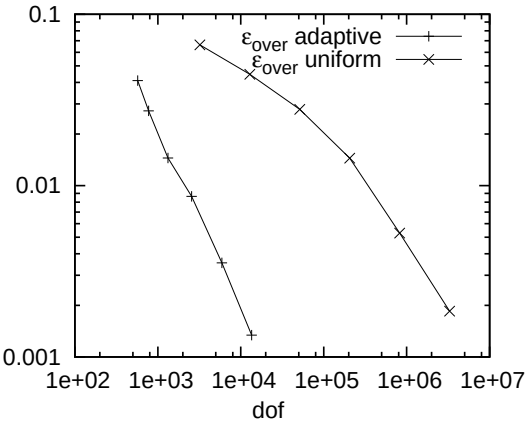

FIGURE 20. MEASURE $\varepsilon_{\text{over}}(t^n = 1.5)$ FOR VARIOUS Nr AND $|\mathfrak{n}|_{\max}$ AS A FUNCTION OF DEGREES OF FREEDOM.

adaptive method than for the non-adaptive method. For instance, to achieve a value of 10^{-2} for $\varepsilon_{\text{over}}$, the number of degrees of freedom needed for the adaptive method can be roughly two orders of magnitude smaller than that for the non-adaptive one. These savings in terms of degrees of freedom yield significant savings in terms of computational time.

Finally, we compare the adaptive method to the non-adaptive one through the following error measures:

$$\varepsilon^2_{\text{ex}}(t^n = 1.5) := \frac{\Delta x}{M} \sum_{i=1}^{\text{Nc}} \sum_{j=1}^{M} \Big(U_i^n(\xi^{(j)}) - U^{\text{ex}}(x_i, t^n, \xi^{(j)}) \Big)^2, \quad (53)$$

$$\varepsilon^2_{\text{MC}}(t^n = 1.5) := \frac{\Delta x}{M} \sum_{i=1}^{\text{Nc}} \sum_{j=1}^{M} \Big(U_i^n(\xi^{(j)}) - U^{\text{MC}}(x_i, t^n, \xi^{(j)}) \Big)^2, \quad (54)$$

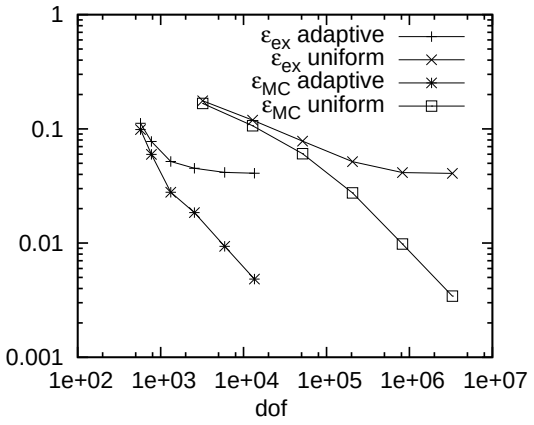

FIGURE 21. ERRORS ε_{ex} AND ε_{MC} AT $t^n = 1.5$ FOR VARIOUS Nr AND $|\mathtt{n}|_{\max}$ AS A FUNCTION OF DEGREES OF FREEDOM.

where $U_i^n(\xi^{(j)})$, $U^{\text{ex}}(x_i,t^n,\xi^{(j)})$, and $U^{\text{MC}}(x_i,t^n,\xi^{(j)})$ are evaluated for $\xi^{(i)}$ belonging to a random sample set respectively from the stochastic expansion of the computed solution, the exact solution of the deterministic Burgers problem at the cell center x_i and discrete time t^n, and by solving the deterministic discrete Burgers problem. We use a sample set with cardinality $M = 10^5$. These two error measures are represented in Figure 20 as a function of degrees of freedom (note the log scales) for $\text{Nr} = 1,2,3,4,5,6$ and $|\mathtt{n}|_{\max} = 4,6,8,10,12,14$. The errors for the adaptive and non-adaptive methods exhibit a similar decay rate, but the adaptive method achieves a given error level with much less degrees of freedom. We also notice that the error measure ε_{ex} stagnates beyond a certain number of degrees of freedom since the error is then dominated by the space discretization error.

CONCLUSION

We have proposed an adaptive anisotropic strategy in the context of multiresolution analysis for uncertain conservation laws with a locally refined stochastic approximation space depending on space and time. The present results illustrate the ability of the method to deal with nonlinear scalar conservation laws including shocks while achieving significant computational savings owing to the adapted discretization. However, the present adaptive strategy still involves some parts that can be improved, in particular, by considering more advanced enrichment and prediction procedures. These improvements are needed before considering the application to complex uncertain hyperbolic systems.

REFERENCES

[1] Le Maître, O. P., and Knio, O. M., 2010. *Spectral Methods for Uncertainty Quantification with Applications to Computational Fluid Dynamics*. Springer Series in Scientific Computation.

[2] Ghanem, R. G., and Spanos, P. D., 2003. *Stochastic finite elements: a spectral approach*. Dover.

[3] Ge, L., Cheung, K., and Kobayashi, M., 2008. "Stochastic Solution for Uncertainty Propagation in Nonlinear Shallow-Water Equations". *Journal of Hydraulic Engineering*, pp. 1732–1743.

[4] Gottlieb, D., and Xiu, D., 2008. "Galerkin method for wave equations with uncertain coefficients". *Commun. Comput. Phys.*, ***3***(2), pp. 505–518.

[5] Lin, G., Su, C.-H., and Karniadakis, G. E., 2006. "Predicting shock dynamics in the presence of uncertainties". *J. Comput. Phys.*, ***217***(1), pp. 260–276.

[6] Poette, G., Després, B., and Lucor, D., 2009. "Uncertainty quantification for systems of conservation laws". *J. Comput. Phys.*, ***228***(7), pp. 2443–2467.

[7] Tryoen, J., Le Maître, O., Ndjinga, M., and Ern, A., 2010. "Intrusive Galerkin Methods with Upwinding for Uncertain Nonlinear Hyperbolic Systems". *J. Comput. Phys.* In Press, See `http://dx.doi.org/10.1016/j.jcp.2010.05.007`.

[8] Deb, M. K., Babuška, I. M., and Oden, J. T., 2001. "Solution of stochastic partial differential equations using Galerkin finite element techniques". *Comput. Methods Appl. Mech. Engrg.*, ***190***(48), pp. 6359–6372.

[9] Le Maître, O. P., Najm, H. N., Ghanem, R. G., and Knio, O. M., 2004. "Multi-resolution analysis of Wiener-type uncertainty propagation schemes". *J. Comput. Phys.*, ***197***(2), pp. 502–531.

[10] Wan, X., and Karniadakis, G. E., 2006. "Multi-element generalized polynomial chaos for arbitrary probability measures". *SIAM J. Sci. Comput.*, ***28***(3), pp. 901–928 (electronic).

[11] Tryoen, J., Le Maître, O., Ndjinga, M., and Ern, A., 2010. "Roe Solver with Entropy Corrector for Uncertain Nonlinear Hyperbolic Systems". *J. Comput. Appl. Math.* To appear, See `http:/hal.archives-ouvertes.fr`, Preprint 00444845.

[12] Cohen, A., Müller, S., Postel, M., and Kaber, S. M., 2002. "Fully adaptive multiresolution schemes for conservation laws". *Math. Comp.*, ***72***, pp. 183–225.

[13] Cohen, A., Dahnem, W., and DeVore, R., 2004. "Adaptive wavelet techniques in numerical simulation". *Encyclopedia of Computational Mechanics*, ***1***, pp. 157–197.

[14] Alpert, B., 1993. "A class of bases in L_2 for the sparse representation of integral operators". *J. Math. Anal.*, ***24***, pp. 246–262.

[15] Le Maître, O. P., Najm, H. N., Pébay, P. P., Ghanem, R. G., and Knio, O. M., 2007. "Multi-resolution-analysis scheme for uncertainty quantification in chemical systems". *SIAM J. Sci. Comput.*, ***29***(2), pp. 864–889.